LETTER

Autocatalytic, bistable, oscillatory networks of biologically relevant organic reactions

Sergey N. Semenov[1], Lewis J. Kraft[1], Alar Ainla[1], Mengxia Zhao[1], Mostafa Baghbanzadeh[1], Victoria E. Campbell[1], Kyungtae Kang[1], Jerome M. Fox[1] & George M. Whitesides[1,2,3]

Networks of organic chemical reactions are important in life and probably played a central part in its origin[1–3]. Network dynamics regulate cell division[4–6], circadian rhythms[7], nerve impulses[8] and chemotaxis[9], and guide the development of organisms[10]. Although out-of-equilibrium networks of chemical reactions have the potential to display emergent network dynamics[11] such as spontaneous pattern formation, bistability and periodic oscillations[12–14], the principles that enable networks of organic reactions to develop complex behaviours are incompletely understood. Here we describe a network of biologically relevant organic reactions (amide formation, thiolate–thioester exchange, thiolate–disulfide interchange and conjugate addition) that displays bistability and oscillations in the concentrations of organic thiols and amides. Oscillations arise from the interaction between three subcomponents of the network: an autocatalytic cycle that generates thiols and amides from thioesters and dialkyl disulfides; a trigger that controls autocatalytic growth; and inhibitory processes that remove activating thiol species that are produced during the autocatalytic cycle. In contrast to previous studies that have demonstrated oscillations and bistability using highly evolved biomolecules (enzymes[15] and DNA[16,17]) or inorganic molecules of questionable biochemical relevance (for example, those used in Belousov–Zhabotinskii-type reactions)[18,19], the organic molecules we use are relevant to metabolism and similar to those that might have existed on the early Earth. By using small organic molecules to build a network of organic reactions with autocatalytic, bistable and oscillatory behaviour, we identify principles that explain the ways in which dynamic networks relevant to life could have developed. Modifications of this network will clarify the influence of molecular structure on the dynamics of reaction networks, and may enable the design of biomimetic networks and of synthetic self-regulating and evolving chemical systems.

Figure 1 summarizes the network of organic reactions that we used to assemble our model system. All of these reactions are nearly quantitative, and the structure of their reactants can be varied by synthesis to control the rates of reactions. Thiols and thioesters, which are central to these reactions, are important in many biological processes (for example, the formation of disulfide bonds in proteins, transformations involving coenzyme-A, the reduction of oxidized molecules by glutathione[20], the synthesis of polyketides[21] and the non-ribosomal synthesis of peptides[21]) and, hence, might represent reactions that enabled life to emerge on the early Earth[22].

To control the dynamics of these processes, we constructed a modular chemical reaction network, shown schematically in control-theoretic terms[23] in Fig. 1a. A 'trigger' produces an initial chemical signal, and an 'auto-amplifier' amplifies this signal, which may or may not be suppressed by inhibition. To keep the reactions out of equilibrium—and, thus, to enable the self-organization of reactions by communication through concentrations of reactants and products—we used

a continuously stirred tank reactor (CSTR) to mix reactants and products, while allowing a flux of species into and out of the network over time. A biological cell has some conceptual analogies to a micro-metre-scale, diffusively mixed tank reactor. The dynamic behaviour of this system—especially bistability and oscillations—reflects the balances of triggering, auto-amplification and inhibition.

We first constructed a chemical network that is capable of auto-amplification using thiols and thioesters (Fig. 1b). The starting components of the network are cystamine (CSSC, **3**) and L-alanine ethyl thioester (AlaSEt, **2**). Trace amounts of cysteamine (CSH, **1**) are generated as follows: AlaSEt slowly hydrolyses, generating alanine (**8**) and ethanethiol (EtSH, **4**); EtSH then reacts with CSSC via thiolate–disulfide interchange[24], yielding disulfide **6** and CSH. With CSH present, self-amplification occurs through two steps: (i) CSH reacts rapidly with AlaSEt by thiolate–thioester exchange and intramolecular rearrangement (Kent ligation)[25], yielding two thiols, EtSH and L-alanine mercaptoethyl amide (**5**); and (ii) these two thiols then undergo thiolate–disulfide interchange with CSSC, yielding two molecules of CSH (and disulfides **6** and **7**). Because one molecule of CSH generates two molecules of CSH (a multiplication by two), this network proceeds autocatalytically; hereafter, we refer to it as an 'autocatalytic thiol network'.

We tested this autocatalytic thiol network in a batch reactor (in 500 mM phosphate buffer at pH 7.5). The curve showing the formation of alanine amides (**5**, **7**, **11**, **12** and **13**) from the reaction of AlaSEt and CSSC has two attributes that are consistent with autocatalysis (Fig. 2a): it is sigmoidal in shape and the addition of β-mercaptoethanol eliminates the lag period. The results of numerical simulations agree well with experimental results (Extended Data Fig. 1e and Methods). Production of thiols (CSH, **5** and EtSH) also follows autocatalytic kinetics (Extended Data Fig. 1f). Therefore, this system provides a kinetically simple, well-defined autocatalytic reaction—with reactants that can be easily varied structurally by synthesis—based on thiols. Autocatalytic reactions are important in life and play an important part in evolution[26].

Having developed the autocatalytic reaction system, we focused on developing a set of reactions to control the onset of exponential growth of organic thiols (RSH) (the timing of the trigger). The mechanism outlined in Fig. 1b suggests that a molecule that is capable of rapidly reacting with and, hence, rapidly removing free thiols might delay autocatalytic growth until that molecule is itself depleted by reaction. We hypothesized that the addition of maleimide, which reacts extremely rapidly with thiolates (in comparison to all other rates of reaction in the autocatalytic thiol network), would prevent the formation of **5** and thus prevent auto-amplification of thiols until it is completely consumed. Therefore, in a reaction of AlaSEt, CSSC and maleimide, molecules of EtSH—a free thiol generated by the hydrolysis of AlaSEt—will react with and eventually consume maleimide, at which point the autocatalytic formation of CSH can proceed (Fig. 1b).

To test the ability of maleimide to delay autocatalytic growth, we added 5 mol% of this molecule to a mixture of CSSC and AlaSEt (in

[1]Department of Chemistry and Chemical Biology, Harvard University, 12 Oxford Street, Cambridge, Massachusetts 02138, USA. [2]Kavli Institute for Bionano Inspired Science and Technology, School of Engineering and Applied Sciences, Harvard University, 29 Oxford Street, Cambridge, Massachusetts 02138, USA. [3]Wyss Institute for Biologically Inspired Engineering, Harvard University, 60 Oxford Street, Cambridge, Massachusetts 02138, USA.
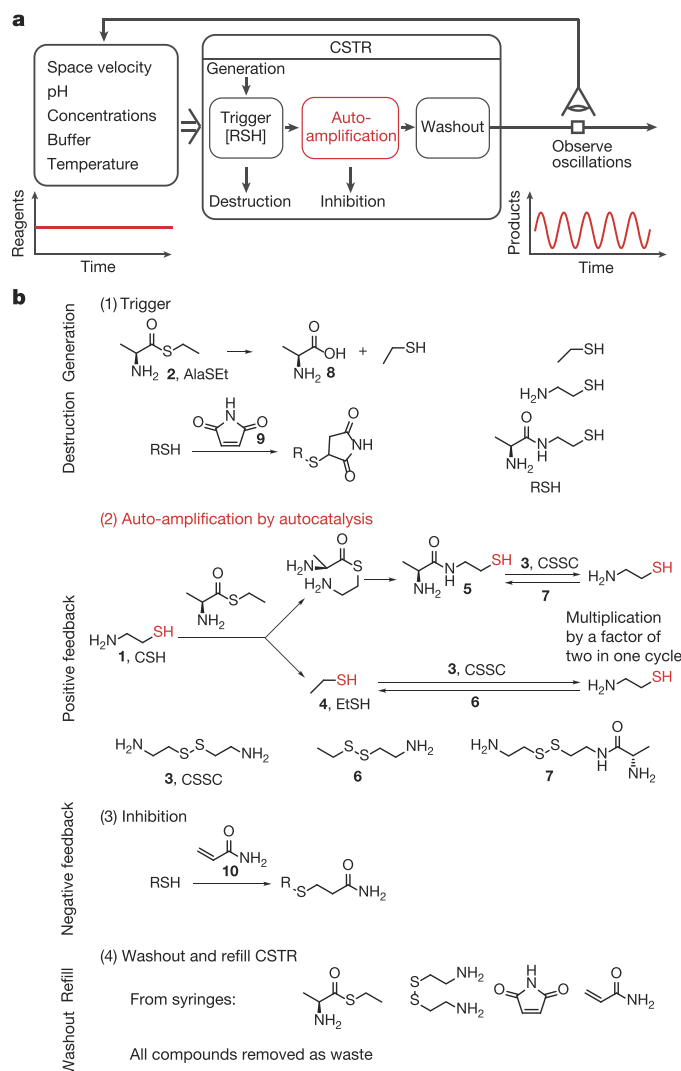
Figure 1 | Overview of the network of organic reactions. a, A diagram showing the inputs and outputs of a continuously stirred tank reactor (CSTR). Input (control) parameters include reactor space velocity (flow rate/reactor volume), pH, concentrations of the chemical species, buffer composition and temperature. The output is the thiol concentration [RSH], which changes with time. Inside the CSTR, the trigger is a balance between the generation and the destruction of RSH, which regulates the auto-amplification of RSH. Inhibition and washout remove RSH. **b**, Reaction schemes describing the elements of the diagram in **a** that collectively lead to oscillations. (1) Trigger: slow production of RSH by hydrolysis of the thioester, in combination with removal of RSH by reaction with maleimide. (2) Auto-amplification by autocatalysis: RSH provides a positive feedback loop via thiol–disulfide exchange with CSSC, followed by native chemical ligation with AlaSEt (direct attack of CSSC on AlaSEt is negligible; see Extended Data Fig. 1a–d). (3) Inhibition: removal of RSH by conjugate addition to an excess of acrylamide provides a negative feedback loop. (4) Washout and refill of CSTR: AlaSEt, CSSC, maleimide and acrylamide are supplied from syringes; all compounds are removed as effluent (see Extended Data Fig. 2 for omitted exchange reactions and Extended Data Table 1 for details of protonation equilibria). All compounds are represented in their electrically neutral forms for simplicity. Autocatalytic module and autocatalytic species are highlighted in red.

batch), and used proton nuclear magnetic resonance (¹H NMR) to monitor both the production of alanine amides and the disappearance of maleimide (Fig. 2b and Extended Data Fig. 3a–c). The production of alanine amides does not proceed until maleimide is consumed, at which point it proceeds autocatalytically.

In a CSTR, autocatalytic reactions can become bistable[27]. In flow systems, bistability often manifests itself through hysteresis; concentrations

of reaction intermediates, which are determined by flow rates, do not return to their original values when flow rates are changed and then changed back. To test our reaction network under flow conditions, we constructed a small CSTR and connected it to a spectrophotometer to continuously monitor the total concentration of thiols in the system (Fig. 3, Extended Data Fig. 4). The molecules fed into this CSTR included AlaSEt, CSSC and maleimide.

Numerical simulations suggested that space velocities (defined as the ratio of the flow rate and the reactor volume and given in units of per second) in the range 0.0001–0.01 s⁻¹ would produce hysteresis (see Extended Data Fig. 5a–c). To test the result of these simulations, we monitored the total concentration of thiols during stepwise changes in space velocity within the predicted range. We started from a low flow rate, ramped up to a high flow rate, and then returned to the low flow rate (Fig. 4a). High thiol concentrations generated through self-amplification (of CSH) require the space velocities to be lowered to $\leq 0.0005\,\mathrm{s}^{-1}$ to activate the autocatalytic pathway. The system transitions out of the self-amplifying state when the space velocity is $\geq 0.006\,\mathrm{s}^{-1}$ (Fig. 4b). These limits make qualitative sense: self-amplification requires maleimide to be removed from the CSTR (via reactions with free thiols—or, more exactly, thiolate anions—or via transport out of the CSTR through the outlet port) more rapidly than it is added through the inlet port; the termination of self-amplification, once it has started, requires free thiols to be removed from the CSTR by transport out of the outlet port more rapidly than they are produced (via autocatalysis). An increase in maleimide concentration lowers the limiting flow rates for bistability (Fig. 4c; Extended Data Fig. 5d–f), as the model predicts. This chemical reaction network illustrates a general way to convert any quadratic autocatalytic system (and perhaps, any system capable of exponential amplification) into a bistable switch by combining this autocatalysis with linear generation and quantitative sequestration of the self-amplifying species.

It has been shown that bistable systems can give rise to oscillations in the presence of an inhibition reaction that slowly (relative to a production reaction) removes the self-amplifying species[13,27,28]. In our system, we chose acrylamide as an inhibitor, because this molecule reacts more slowly with thiols than any other molecule in the reaction network. When we tested this system with acrylamide in batch, it exhibited a single oscillation (that is, one peak) in the concentration of free thiols (Fig. 2c; Extended Data Fig. 3d, e). NMR analysis (Fig. 2d) shows that the oscillation is not triggered until the maleimide is removed. In addition, it is apparent that AlaSEt is depleted during the oscillation.

Using a combination of numerical simulations and experiments in the CSTR under different flow rates (inputs were AlaSEt, maleimide and acrylamide), we identified conditions under which the addition of acrylamide, present in excess, would produce sustained oscillations in RSH (Fig. 4d; Extended Data Fig. 6). Each oscillation arises from three steps (Fig. 4e and Methods): (i) the trigger sets up a delay for auto-amplification of the autocatalytic thiol species; (ii) autocatalytic growth competes with inhibition of thiols by reaction with acrylamide, thus depleting the thioester AlaSEt; (iii) the thioester AlaSEt (and other reagents) is recharged by flow into the CSTR.

To determine how changes in flow rate effect oscillations, we examined the influence of flow rate on the stability, period and amplitude of oscillations. Sustained oscillations occurred for space velocities between $1.4 \times 10^{-4}\,\mathrm{s}^{-1}$ and $2.7 \times 10^{-4}\,\mathrm{s}^{-1}$ (Fig. 4f; Extended Data Fig. 7). Increasing the space velocity to $2.8 \times 10^{-4}\,\mathrm{s}^{-1}$ resulted in a sudden loss of oscillations, and decreasing it to $1.2 \times 10^{-4}\,\mathrm{s}^{-1}$ resulted in damped oscillations. The period increased nonlinearly with space velocity (Fig. 4f); by contrast, the amplitude increased linearly (Fig. 4g).

To explain the trends in period and amplitude of the oscillations, and the nature of the bifurcations at low and high limiting space velocities, we constructed a simple kinetic model (Fig. 4h) that enables qualitative analysis of dynamic behaviours in our oscillating network. This model simplifies the autocatalytic thiol network to bimolecular autocatalytic
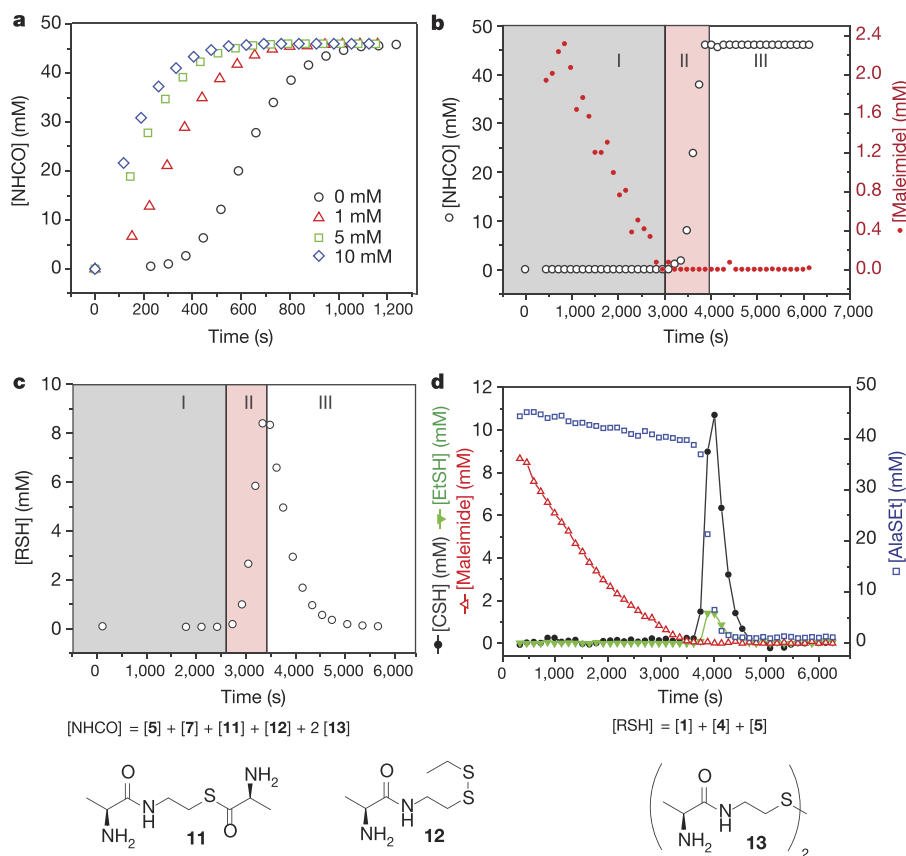
Figure 2 | Summary of the batch kinetic studies of the organic reaction network. a, Experiments showing elimination of the lag period in the autocatalytic reaction (46 mM AlaSEt with 46 mM CSSC) by addition of various concentrations of β-mercaptoethanol (see legend). To quantify the kinetics of this reaction, we followed the production of amide derivatives of alanine using ^{1}H NMR spectroscopy. The chemical shift of a proton linked to the α-carbon of ʟ-alanine is different for AlaSEt (4.05 p.p.m.) and alanine amides (**5, 7, 11, 12** and **13**; the chemical shifts of 3.85 p.p.m. for these five compounds are indistinguishable). Reaction conditions: D_2O, 500 mM phosphate buffer pH 7.5, 25 °C. **b,** To quantify the kinetics of the trigger (the reaction of 46 mM AlaSEt with 46 mM CSSC in the presence of 2.31 mM maleimide), we again followed the production of amide derivatives of alanine and maleimide by ^{1}H NMR. Region I indicates the period of delay regulated by the trigger, region II indicates a period of autocatalytic production of RSH, and region III indicated a period in

which AlaSEt is depleted and so no further reactions occur. See Extended Data Fig. 3a–c for additional experiments. Reaction conditions are the same as in **a**. **c,** To quantify the kinetics of a single oscillation in [RSH] (the reaction of 46 mM AlaSEt, 92 mM CSSC, 7.66 mM maleimide and 282 mM acrylamide), we monitored [RSH] using Ellman's reagent (Extended Data Fig. 4). Regions I and II correspond to the trigger and autocatalytic regimes, respectively; region III corresponds to a period of inhibition by conjugate addition of RSH to acrylamide. Reaction conditions: H_2O, 1 M phosphate buffer pH 8.0, 25 °C. **d,** Time dependence of [AlaSEt], [CSH], [EtSH] and [maleimide] during a single oscillation by ^{1}H NMR. Initial concentrations for the reaction: D_2O, 1 M phosphate buffer pH 8.0, 25 °C, [AlaSEt] = 47 mM, [CSSC] = 92 mM, [maleimide] = 10 mM, [acrylamide] = 320 mM. Exact definitions of total concentration of amides ([NHCO]) and total concentration of thiols ([RSH]) are shown below the plots.
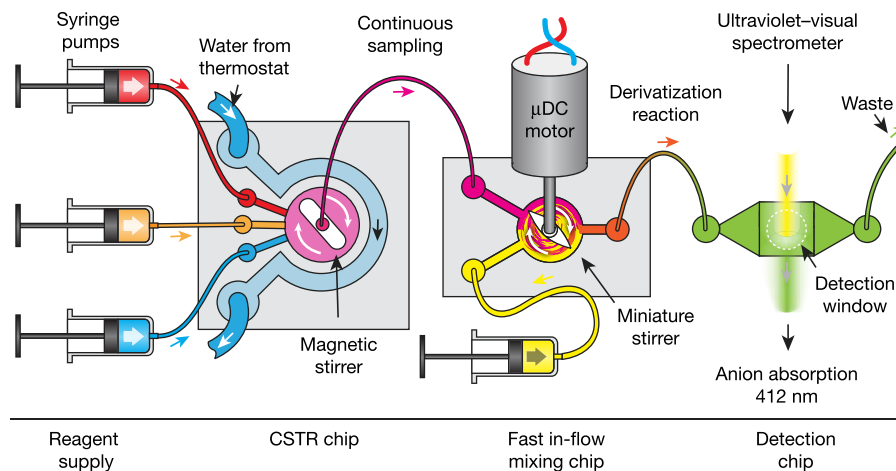

Figure 3 | Schematic representation of the CSTR experimental set-up. In this set-up, syringe pumps feed reactants to the inlet ports of the CSTR, where they mix and react (red, CSSC in a phosphate buffer of pH 7.5 or 8; orange, AlaSEt in Milli-Q water; blue, maleimide and/or acrylamide in Milli-Q water). For continuous sampling, a tube connected to the outlet

port of the CSTR takes the effluent (products and reactants) to a fast in-flow mixing detection chip powered by a μDC (micro direct current) motor. In this chip, RSH reacts with 5,5′-dithiobis-(2-nitrobenzoic acid) and forms 4-nitro-3-carboxy-thiophenolate anion, which is detected by absorption at 412 nm using an ultraviolet–visual spectrometer.
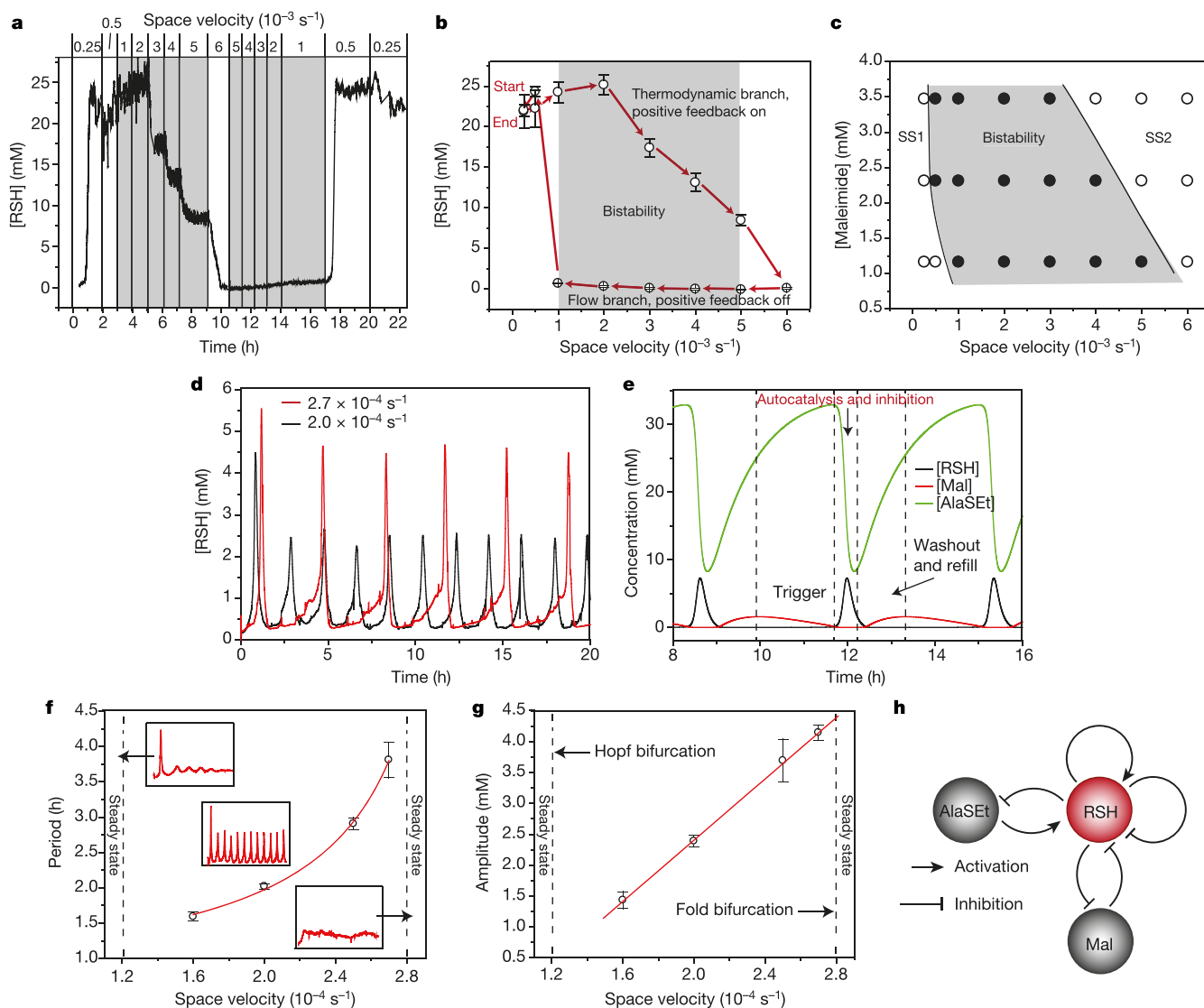
Figure 4 | The network of organic reactions displays bistability and sustained oscillations under flow. a, Representative experimental trace showing changes in [RSH] over time as a result of changes in space velocity. **b**, Hysteresis curve derived from steady-state [RSH] in the trace presented in **a** (see Methods for additional conditions). Error bars correspond to standard deviations that were calculated from data points ($n > 100$) in the time intervals that were used to determine the steady-state values of [RSH] for each space velocity. **c**, Phase plot reconstructed from three separate experiments using different maleimide concentrations. The open and closed circles indicate single steady states and bistable points, respectively. SS1, steady state 1 (autocatalysis is on); SS2, steady state 2 (autocatalysis is off). Experimental conditions: H_2O, 500 mM phosphate buffer pH 7.5, 25 °C, [AlaSEt] = 46 mM; [CSSC] = 92 mM, [maleimide] = 1.16 mM, 2.31 mM and 3.47 mM, space velocities of $(0.25–6) \times 10^{-3}\,s^{-1}$. Grey shading in **a**–**c** indicates regions of bistability. **d**, Experimental data showing sustained oscillations at two different space velocities, $2.7 \times 10^{-4}\,s^{-1}$ (red line) and $2.0 \times 10^{-4}\,s^{-1}$ (black line), using the following reactants: [AlaSEt] = 47 mM,

[CSSC] = 92 mM, [maleimide] = 10 mM, [acrylamide] = 320 mM in 1 M phosphate buffer pH 8.0, 28 °C. **e**, Simulations that show an example of the evolution of the concentration of key species (RSH, black; maleimide, red; AlaSEt, green) during oscillations (see Extended Data Fig. 6a for modelling parameters). **f**, Influence of space velocity on the stability and period of the oscillations. Open circles represent experimental data. The solid line is a hyperbolic fit to the data. Insets show examples of the dynamics of [RSH] in the indicated regions. **g**, The influence of space velocity on the amplitude of oscillations. Open circles represent experimental data. The solid line is a linear fit to the data. Dashed lines in **f** and **g** are the estimated borders for sustained oscillations. Error bars in **f** and **g** correspond to 90% confidence intervals calculated using Student's t-test (three independent experiments for each space velocity). Separate plots for each experimental examination of oscillations are provided in Extended Data Fig. 7. **h**, Simplified depiction of the overall network of organic reactions; 'Mal.', maleimide. Arrow heads and blunt arrow heads represent activation and inhibition, respectively.

production of thiols from thioester, and considers the concentrations of CSSC and acrylamide ([CSSC] and [acrylamide]) as constants:

$$\frac{dA}{dt} = k_1 SA - k_2 IA - k_3 A - k_0 A + k_4 S$$

$$\frac{dI}{dt} = k_0 I_0 - k_0 I - k_2 IA \qquad (1)$$

$$\frac{dS}{dt} = k_0 S_0 - k_0 S - k_4 S - k_1 SA$$

Here, $A = $ [RSH], $I = $ [maleimide], $S = $ [AlaSEt], I_0 and S_0 are the concentrations of maleimide and AlaSEt fed into the reactor, respectively, k_{1-4} are rate constants and k_0 is the space velocity. Linear stability analysis[13] of this model shows that increasing k_0 from low to high values causes two transitions. First, the system transitions from having a stable focus (damped oscillations) to a stable orbit (sustained oscillations) via an Andronov–Hopf bifurcation[29]. Second, the system transitions from having a stable orbit to a single stable equilibrium (a stable 'node'—an equilibrium in which the system, when perturbed, returns directly to the stable state, as opposed to orbiting around it)

via a saddle-node or fold bifurcation[29] (see Extended Data Fig. 8a and Methods). Further analysis of this model shows that lowering the concentration of maleimide fed into the reactor (I_0) results in a transition from oscillatory to bistable behaviour (see phase plot in Extended Data Fig. 8b). Indeed, experiments with $I_0 = 4\,\text{mM}$ (all other parameters are the same as those in experiments on oscillations) demonstrated the predicted bistable behaviour of the system at space velocities ranging from $0.0015\,\text{s}^{-1}$ to $0.005\,\text{s}^{-1}$ (Extended Data Fig. 8c).

Our experiments show that we have successfully converted a bistable organic reaction network into an oscillatory network with two experimentally accessible and biologically relevant classes of bifurcations. Systematically designed chemical oscillators are rare. Notable examples are enzymatic[15], pH[30], DNA[16,17] and redox oscillators;[28] here, we have demonstrated a class of chemical oscillators based on thiols. This system is unique in that it has characteristics that make it relevant to the discussion of the spontaneous formation of networks from types of molecules relevant to metabolism, to other dynamic networks of organic reactions and perhaps to the origin of life.

This network, which requires only four components (a thioester, a disulfide of a β-aminothiol, a kinetically rapid and irreversible thiol inhibitor, and a slow and irreversible thiol inhibitor), can be varied via structural modifications of the constituent organic molecules; this flexibility in structures offers the potential to explore the evolution and functional design of dynamic networks. The complex behaviour of this simple network of organic reactions illustrates four ideas that are important when considering the emergence of complexity in dynamic networks of chemical reactions. First, our network demonstrates the ability of a simple set of reactants to produce emergent behaviour when feedback is present. Second, it shows 'memory' in the sense that the system is hysteretic and thus encodes information about its past in the concentrations of molecules in the network; in discussions of the origin of life, memory is usually attributed to sequences of bases in replicating molecules of RNA, or its precursors, and alternative forms of memory in dynamic networks broaden its possible origins. Third, our network is compatible with the types of behaviour envisioned[22] in a proposal for a 'thioester' basis for the origin of life; this compatibility reinforces the relevance of this proposal. Finally, our network suggests that the complex regulatory dynamics generally associated with cellular function (for example, threshold-based behaviours and circadian rhythms) might, in principle, have arisen spontaneously before cellular life and, perhaps most importantly, before enzymatic catalysis.

1. Dyson, F. J. A model for the origin of life. *J. Mol. Evol.* **18**, 344–350 (1982).
2. Nghe, P. *et al.* Prebiotic network evolution: six key parameters. *Mol. Biosyst.* **11**, 3206–3217 (2015).
3. Patel, B. H., Percivalle, C., Ritson, D. J., Duffy, C. D. & Sutherland, J. D. Common origins of RNA, protein and lipid precursors in a cyanosulfidic protometabolism. *Nat. Chem.* **7**, 301–307 (2015).
4. Tyson, J. J., Chen, K. C. & Novak, B. Sniffers, buzzers, toggles and blinkers: dynamics of regulatory and signaling pathways in the cell. *Curr. Opin. Cell Biol.* **15**, 221–231 (2003).
5. Ferrell, J. E., Tsai, T. Y. C. & Yang, Q. O. Modeling the cell cycle: why do certain circuits oscillate? *Cell* **144**, 874–885 (2011).
6. Tyson, J. J. Modeling the cell-division cycle: cdc2 and cyclin interactions. *Proc. Natl Acad. Sci. USA* **88**, 7328–7332 (1991).
7. Goldbeter, A. A model for circadian oscillations in the *Drosophila* period protein (PER). *Proc. R. Soc. Lond. B* **261**, 319–324 (1995).
8. FitzHugh, R. Impulses and physiological states in theoretical models of nerve membrane. *Biophys. J.* **1**, 445–466 (1961).
9. Laub, M. T. & Loomis, W. F. A molecular network that produces spontaneous oscillations in excitable cells of dictyostelium. *Mol. Biol. Cell* **9**, 3521–3532 (1998).
10. Lander, A. D. Pattern, growth, and control. *Cell* **144**, 955–969 (2011).
11. Hazen, R. M., Griffin, P. L., Carothers, J. M. & Szostak, J. W. Functional information and the emergence of biocomplexity. *Proc. Natl Acad. Sci. USA* **104**, 8574–8581 (2007).
12. Whitesides, G. M. & Ismagilov, R. F. Complexity in chemistry. *Science* **284**, 89–92 (1999).
13. Epstein, I. R. & Pojman, J. A. *An introduction to Nonlinear Chemical Dynamics: Oscillations, Waves, Patterns, and Chaos* Chs 2 and 4, 17–47 and 62–83 (Oxford Univ. Press, 1998).
14. Grzybowski, B. A. *Chemistry in Motion: Reaction-diffusion Systems for Micro- and Nanotechnology* Chs 1 and 4, 1–12 and 61–90 (Wiley, 2009).
15. Semenov, S. N. *et al.* Rational design of functional and tunable oscillating enzymatic networks. *Nat. Chem.* **7**, 160–165 (2015).
16. Kim, J. & Winfree, E. Synthetic *in vitro* transcriptional oscillators. *Mol. Syst. Biol.* **7**, 465 (2011).
17. Montagne, K., Plasson, R., Sakai, Y., Fujii, T. & Rondelez, Y. Programming an *in vitro* DNA oscillator using a molecular networking strategy. *Mol. Syst. Biol.* **7**, 466 (2011).
18. Belousov, B. P. Periodicheski deistvuyushchaya reaktsia i ee mechanism [in Russian]. In *Sbornik Referatov po Radiatsionni Meditsine* 145–147 (Moscow: Medgiz, 1958).
19. Gyorgyi, L., Turányi, T. & Field, R. J. Mechanistic details of the oscillatory Belousov–Zhabotinskii reaction. *J. Phys. Chem.* **94**, 7162–7170 (1990).
20. Meister, A. & Anderson, M. E. Glutathione. *Annu. Rev. Biochem.* **52**, 711–760 (1983).
21. Fischbach, M. A. & Walsh, C. T. Assembly-line enzymology for polyketide and nonribosomal peptide antibiotics: logic, machinery, and mechanisms. *Chem. Rev.* **106**, 3468–3496 (2006).
22. De Duve, C. *Singularities: Landmarks on the Pathways of Life* Ch. 6, 54–66 (Cambridge Univ. Press, 2005).
23. LeDuc, P. R., Messner, W. C. & Wikswo, J. P. How do control-based approaches enter into biology? *Annu. Rev. Biomed. Eng.* **13**, 369–396 (2011).
24. Houk, J. & Whitesides, G. M. Structure reactivity relations for thiol disulfide interchange. *J. Am. Chem. Soc.* **109**, 6825–6836 (1987).
25. Dawson, P. E., Muir, T. W., Clarklewis, I. & Kent, S. B. H. Synthesis of proteins by native chemical ligation. *Science* **266**, 776–779 (1994).
26. Bissette, A. J. & Fletcher, S. P. Mechanisms of autocatalysis. *Angew. Chem. Int. Ed.* **52**, 12800–12826 (2013).
27. Boissonade, J. & De Kepper, P. Transitions from bistability to limit cycle oscillations. Theoretical analysis and experimental evidence in an open chemical system. *J. Phys. Chem.* **84**, 501–506 (1980).
28. De Kepper, P., Epstein, I. R. & Kustin, K. A systematically designed homogeneous oscillating reaction: the arsenite–iodate–chlorite system. *J. Am. Chem. Soc.* **103**, 2133–2134 (1981).
29. Kuznetsov, I. U. A. *Elements of Applied Bifurcation Theory* 3rd edn, Ch. 3, 77–115 (Springer, 2004).
30. Kovacs, K., McIlwaine, R. E., Scott, S. K. & Taylor, A. F. An organic-based pH oscillator. *J. Phys. Chem. A* **111**, 549–551 (2007).

Author Contributions S.N.S. and G.M.W. conceived the research and designed the experiments. S.N.S., L.J.K., A.A., M.Z., V.E.C., M.B. and K.K. performed the experiments and analysed the data. S.N.S., L.J.K., A.A. and J.M.F. performed the computational simulations. S.N.S., L.J.K., J.M.F., V.E.C. and G.M.W. wrote the manuscript.

Author Information Reprints and permissions information is available at www.nature.com/reprints. The authors declare no competing financial interests. Readers are welcome to comment on the online version of the paper. Correspondence and requests for materials should be addressed to G.M.W. (gwhitesides@gmwgroup.harvard.edu).

Reviewer Information *Nature* thanks A. Bissette, S. Fletcher and the other anonymous reviewer(s) for their contribution to the peer review of this work.

METHODS

Synthesis. *General.* Unless otherwise stated, all starting materials were obtained commercially and were used without further purification. Nuclear magnetic resonance (NMR) spectra were measured on a Varian INOVA I-500 spectrometer at 500 MHz for ^{1}H and 125.8 MHz for ^{13}C(^{1}H) or on a Varian INOVA I-400 spectrometer at 400 MHz for ^{1}H. The chemical shifts for ^{1}H and ^{13}C are given in parts per million (p.p.m.) relative to TMS, and calibrated using the residual ^{1}H peak of the solvent; $\delta = 7.26$ for CDCl$_3$ and $\delta = 4.79$ for D$_2$O in ^{1}H NMR, and $\delta = 77.2$ for CDCl$_3$ in ^{13}C NMR. Fourier transform infrared spectroscopy (FT-IR) spectra were recorded on a Bruker TENSOR 27 spectrometer fitted with an attenuated total reflectance (ATR) cell.

N-Boc-L-alanine ethyl thioester (BocAlaSEt). N-(3-dimethylaminopropyl)-N'-ethylcarbodiimide hydrochloride (EDC·HCl) (5.57 g, 29.0 mmol) was added to a stirred solution of N-Boc-L-alanine (4.00 g, 26.4 mmol) and ethanethiol (2.45 ml, 34.4 mmol) dissolved in 25 ml of DMF at 0 °C under an argon atmosphere. After allowing the reaction to proceed for 1 h at 0 °C, the mixture was left at room temperature overnight. DMF was removed *in vacuo*. The residue was dissolved in ethyl acetate (50 ml), washed with de-ionized water (2 × 5 ml), dried over Na$_2$SO$_4$ and concentrated on the rotary evaporator. The crude product was purified by column chromatography (SiO$_2$, CH$_2$Cl$_2$:EtOAc 95:5, $R_f \approx 0.5$). Yield, 63% (3.90 g, 16.74 mmol). ^{1}H NMR (400 MHz, CDCl$_3$): $\delta = 4.38$ p.p.m. (m, 1H, NHC*H*), 2.87 p.p.m. (q, $^3J_{H-H} = 7.4$ Hz, 2H, SC*H$_2$*), 1.45 p.p.m. (s, 9H, C(C*H$_3$*)$_3$), 1.37 p.p.m. (d, 3H, $^3J_{H-H} = 7.2$ Hz, NHCHC*H$_3$*) 1.25 p.p.m. (t, $^3J_{H-H} = 7.4$ Hz, 2H, SCH$_2$C*H$_3$*) (the superscript 3 indicates the number of covalent bonds through which the coupling occurs).

L-alanine ethyl thioester trifluoroacetic salt (AlaSEt·TFA). Trifluoroacetic acid (TFA) (12 ml) was added dropwise to a solution of N-Boc-L-alanine ethyl thioester (1.25 g, 5.4 mmol) in dichloromethane (CH$_2$Cl$_2$) (12 ml) at 0 °C. The reaction was stirred at 0 °C for 15 min and then at room temperature for 45 min. The solvents were removed *in vacuo*, and the residue was dissolved in toluene (5 ml). Removal of toluene *in vacuo* yielded pure L-alanine ethyl thioester trifluoroacetic salt (AlaSEt·TFA) as a white solid (96% pure, TFA is a major admixture). Its purity was determined by NMR with L-alanine as an internal standard. Yield, 97% (1.30 g, 5.3 mmol). ^{1}H NMR (500 MHz, D$_2$O): $\delta = 4.18$ p.p.m. (q, $^3J_{H-H} = 7.5$ Hz, NHC*H*), 2.85 p.p.m. (m, 2H, SC*H$_2$*), 1.43 p.p.m. (d, 3H, $^3J_{H-H} = 7$ Hz, NHCHC*H$_3$*) 1.11 p.p.m. (t, $^3J_{H-H} = 7.5$ Hz, 3H, SCH$_2$C*H$_3$*).

Batch kinetic experiments. *General.* The kinetic experiments were performed at 25 °C in a 500 mM phosphate buffer (pH 7.5) solution in D$_2$O by monitoring the change in the ^{1}H NMR spectra. We calculated the progress of the Kent ligation reaction by integrating the ^{1}H NMR signal of the proton linked to the α-carbon of L-alanine derivatives at $\delta = 3.85$ p.p.m. (α-protons of **5**, **7**, **11**, **12** and **13**). The concentrations of the starting materials were calculated by setting the total integral of alanine α-protons equal to the starting concentration of AlaSEt. The total thiol concentration ([CSH] + [EtSH] + [**5**]) in the batch experiments was determined with Ellman's reagent (5,5′-dithiobis-2-nitrobenzoic acid) (0.5 mM, phosphate buffer pH 7, 100 mM). A 7.5 μl sample was added to the Ellman's solution and the absorbance of this solution was measured by ultraviolet–visible spectroscopy after 1 min of incubation. We calculated thiol concentration from absorbance using a calibration curve (Extended Data Fig. 4a). In all plots, we show total concentration of all protonated/deprotonated forms; see Extended Data Table 1 for details of protonation equilibria[31–33].

Reaction between AlaSEt and cystamine (CSSC). First, we dissolved cystamine hydrochloride (CSSC·2HCl) (40.2 mM, 80.5 mM or 161.0 mM solution) in 0.4 ml of 500 mM phosphate buffer (pH 7.5) in D$_2$O and filled the NMR tube with this solution. Second, we dissolved AlaSEt·TFA (107 mM) in 0.3 ml of 500 mM phosphate buffer (pH 7.5) in D$_2$O and mixed it with the CSSC·2HCl solution. Third, we recorded the ^{1}H NMR spectrum every minute (72-s time intervals considering 12 s of acquisition time).

Reaction between AlaSEt and CSSC in the presence of maleimide. We performed experiments as described above. We dissolved CSSC·2HCl (80.5 mM) and maleimide (2.0 mM, 4.0 mM or 6.1 mM) in 0.4 ml of 500 mM phosphate buffer (pH 7.5) in D$_2$O and filled the NMR tube with this solution. Thereafter, we dissolved AlaSEt·TFA (107 mM) in 0.3 ml of 500 mM phosphate buffer (pH 7.5) in D$_2$O and mixed it with the first solution. In addition to the progress of Kent ligation, we monitored the disappearance of maleimide by following the disappearance of maleimide proton signals in the ^{1}H NMR spectra. The interval between measurements was 2 min (132-s time intervals considering 12 s of acquisition time).

Reaction between AlaSEt and CSSC in the presence of maleimide and acrylamide. First, we weighted 8.1 mg of AlaSEt·TFA in a 2-ml glass vial containing a stirring bar. Second, we dissolved CSSC·2HCl (92 mM), maleimide (10 mM) and acrylamide (160 mM or 320 mM) in 0.7 ml of 1 M phosphate buffer (pH 8) in H$_2$O. Third, we quickly added the solution to the alanine thioester, shook vigorously, and put it

on the magnetic stir plate. 7.5-μl aliquots of this mixture were used to determine the amount of free thiols at each time point.

Flow experiments. We used two types of flow systems: a flow system with the CSTR, mixing and detection chip made completely from polydimethylsiloxane (PDMS) (set-up 1), and a flow system with a hybrid PDMS/glass CSTR and a detection chip with mechanical mixing (set-up 2). Set-up 1 is simple to fabricate, and was used for the bistability experiments. Set-up 2 is harder to fabricate than set-up 1, but it gave a more stable signal than set-up 1; therefore, it was used for the oscillatory experiments.

Set-up 1 (for bistability experiments). The CSTR had a volume of 250 μl, was made of PDMS, used a built-in temperature control channel, and had three separate inlets. We mounted three syringes on a Harvard PhD 2000 syringe pump and fed the CSTR with reactants via the inlet tubing. The temperature control channel was connected to a thermostatic water bath. The outlet of the CSTR was connected to the microfluidic detection chip. This detection chip had two inlets, a mixing channel and a detection chamber that was 150 μm in height. It served two functions: mixing outgoing flow of the CSTR with Ellman's reagent (5,5′-dithiobis-(2-nitrobenzoic acid)) and providing an optical window for the ultraviolet–visual absorption measurements. The syringe pump supplied the Ellman's reagent via the second inlet (detection chip). Ellman's reagent quantitatively and irreversibly reacted with the free thiols in the reaction mixture releasing an orange-coloured 4-nitro-3-carboxy-thiophenolate that was detected by ultraviolet–visual absorption. To perform ultraviolet–visual absorption measurements, the detection chamber was aligned with collimated light from the Nikon Intensilight C-HGFI and an optic fibre going to the Ocean Optics HP 4000 ultraviolet–visual absorption spectrometer. We detected the intensity of 412-nm light over the course of the experiment. We converted absorbance into the thiol concentration using a calibration curve (Extended Data Fig. 4b). Artefacts from air bubbles passing the detection window were filtered for clarity. All of the pumps were controlled by a MATLAB program that was specifically designed for these experiments (Supplementary Information).

Set-up 2 (for oscillatory experiments). Detection of the oscillations in the oscillatory experiments required three changes in the fluidic system: using glass instead of PDMS as the material for the CSTR, using active instead of passive mixing during the derivatization step and using a glass flow cell coupled to a Cary 60 ultraviolet–visual spectrometer. The glass CSTR ensured no leakage of EtSH by diffusion through PDMS, and also prevented the accumulation of gas bubbles. The active mixing decreased the retention time during the derivatization step, thus reducing the effect of a side reaction between alanine ethyl thioester and Ellman's reagent. (We determined experimentally that, in this set-up, the background reaction with AlaSEt will generate a signal corresponding to an apparent thiol concentration in the range 0.4–0.8 mM for the flow rates and concentrations of reagents that were used in our experiments; apparent rate constant is about 4×10^4 times slower than the reported apparent second-order rate constant of the reaction between Ellman's reagent and β-mercaptoethanol at pH 7; ref. 34.) The use of a ultraviolet–visual spectrometer eliminated any intensity fluctuations from the light source. Absorbance data were converted into total concentration of free thiols using a calibration curve (Extended Data Fig. 4c, d).

The procedure of making a CSTR with a glass body consisted of three steps. In the first step, we fabricated a glass body. We took a Pasteur pipette, fixed it upside-down in a drill press and heated it 13 mm from the bottom end using a hand-held burner (MT-51). Interplay between gravity and surface tension resulted in the formation of a glass neck with thick walls. The neck had an internal diameter of 0.9–1 mm. We cut the pipette 8 mm above the neck. To make an outlet connection for tubing, we put the newly made glass chamber upside-down in a Petri dish filled with PDMS, such that PDMS was up to the middle of the neck, and inserted a needle (outer diameter of 0.9 mm) into the neck from the top. A well-defined channel was formed after the PDMS was cured. In the second step, we fabricated a PDMS body with all of the inlet connections and temperature controller. We placed a brass cylinder (diameter, 6. mm; height, 6.82 mm) and a copper tube (one turn around the cylinder) in the Petri dish, and filled the dish with PDMS up to the top of the cylinder such that the top of the cylinder was not covered by PDMS. After curing, we pulled the PDMS out of the dish and removed the cylinder. We cut the inlet channels on the bottom of the PDMS body, and punched holes for the inlet tubing. In the final step, we plasma-bonded the PDMS body to a glass slide, inserted the glass body into the PDMS body (hole from the brass cylinder), sealed the top with additional PDMS and inserted tubing. It is important to insert the glass body as close as possible to the glass slide; however, the elasticity of the PDMS would not allow for full contact between the glass body and glass slide, which left a gap (0.1–0.2 mm) that was exploited to construct inlet channels for the reactor.

To make a fast in-flow mixing chip, we designed the microfluidic device with mixing chamber (diameter, 3 mm; height, 1 mm; volume, 7 μl) in AutoCAD and 3D-printed moulding master with an Objet Connex 500 3D printer (Stratasys).

After printing, the master was heated in oven at 70 °C overnight to complete the photo-curing process (otherwise, unreacted components inhibit the PDMS curing in a later step). Using syringe needles, we defined liquid ports (0.9 mm outer diameter) and the placement for the impeller shaft (0.6 mm outer diameter). Thereafter, we used a standard PDMS moulding procedure to cast the chip body. After removal from the master, a syringe needle (0.9 mm outer diameter) was inserted into the mixing chamber and a small impeller was grafted into its end. Then, the PDMS body was plasma-bonded to a glass substrate and the syringe needle was sealed with a small drop of PDMS. We connected the shaft of the impeller to a 5-V micro-d.c. motor running at a speed of about 600 r.p.m. Efficient mixing in the outlet channel of the mixing chip was qualitatively confirmed by visual inspection using water and dye.

To construct the glass flow cell, we drilled two holes (18 mm apart) in the glass slide. Next, we cut two 220-mm-thick cover slips in half and glued pairs of these pieces together using photo-curable glue between two thicker pieces. We glued these doubly thick pieces of glass on the glass slide leaving a 1-mm gap between them (the holes should, of course, point to the gap). Next, we attached the top glass slide (without holes) using glue to create the channel. We removed any leftover glue using nitric acid and sodium hydroxide. We then blocked the ends of the channel using epoxy glue, and we made two rectangular-shaped PDMS pieces with holes for tubing in them. Finally, we plasma-bonded these PDMS pieces on top of the holes to make connections for the channel inlet and outlet tubing. We noted that air bubbles could get stuck in the channel when this chip was used at low flow rates ($<1{,}000\,\mu l\,h^{-1}$) and so, to prevent bubbles from getting stuck, we stuffed the inlet with crushed glass capillaries—the broken glass pieces created a hydrophilic net that prevented the continuity of a bubble from the PDMS part of the inlet to the channel.

Bistability experiments. Four syringes were used: syringe 1 (connected to CSTR), AlaSEt·TFA (92 mM) in water; syringe 2 (connected to CSTR), CSSC·2HCl (184 mM) in 1.127 M phosphate buffer pH 7.5; syringe 3 (connected to CSTR), maleimide (19.3 mM, 38.7 mM or 58 mM) in water; syringe 4 (connected to detection chip), 16.6 mM Ellman's reagent in mixture of MeOH:(NaH$_2$PO$_4$ 208 mM) 2:3. Note that Ellman's reagent should be dissolved in MeOH before adding the solution of NaH$_2$PO$_4$. We used the following flow rates (in $\mu l\,min^{-1}$) to construct hysteresis plots. Syringes 1 and 2: 1.7626, 3.525, 7.05, 14.1, 21.15, 28.2, 35.25, 42.3, 35.25, 28.2, 21.15, 14.1, 7.05, 3.525 and 1.7626; syringe 3: 0.225, 0.45, 0.9, 1.8, 2.7, 3.6, 4.5, 5.4, 4.5, 3.6, 2.7, 1.8, 0.9, 0.45 and 0.225; syringe 4: 11.25, 22.5, 45, 90, 135, 180, 225, 270, 225, 180, 135, 90, 45, 22.5 and 11.25.

Oscillatory experiments. Four syringes were used. Syringe 1 (connected to the CSTR), AlaSEt·TFA (140 mM) in water. To obtain a final volume of 3 ml, 104 mg of AlaSEt·TFA (approximate volume 0.1 ml) was dissolved in 2.90 ml of Milli-Q water. Syringe 2 (connected to the CSTR), CSSC·2HCl (276 mM) in 3 M phosphate buffer pH 8 (K$_2$HPO$_4$ and KH$_2$PO$_4$ have to be used to get a 3 M solution). To obtain a final volume of 3 ml, 193.2 mg of CSSC·2HCl was dissolved in 2.85 ml of the buffer. Syringe 3 (connected to the CSTR), maleimide (31 mM) and acrylamide (962 mM) in water. To obtain a final volume of 3 ml, 9 mg of maleimide and 205 mg of acrylamide were dissolved in 2.85 ml of Milli-Q water. Syringe 4 (connected to the mixing chip), 16.6 mM Ellman's reagent in a mixture of MeOH:(NaH$_2$PO$_4$ 208 mM) 2:3. Note that Ellman's reagent should be dissolved in MeOH before adding the solution of NaH$_2$PO$_4$. We used the following flow rates (space velocities in s^{-1}, flow rate for syringes 1, 2 and 3 in $\mu l\,min^{-1}$, flow rate for syringe 4 in $\mu l\,min^{-1}$): $(1.2\times10^{-4}, 36, 324)$, $(1.4\times10^{-4}, 42, 378)$, $(1.6\times10^{-4}, 48, 432)$, $(2.0\times10^{-4}, 60, 540)$, $(2.5\times10^{-4}, 75, 675)$, $(2.7\times10^{-4}, 81, 729)$ and $(2.8\times10^{-4}, 84\,756)$.

Numerical modelling. Numerical modelling was done using COPASI[35] and MATLAB programs. MATLAB numerical models for the oscillatory and bistable networks are described below.

The architectures of our bistable and oscillatory networks are outlined in Extended Data Fig. 9a. Under flow conditions, the evolution of the species in the bistable network over time is governed by the following set of ordinary differential equations:

$$\frac{d[\text{AlaSEt}]}{dt} = -k_L[\text{AlaSEt}][\text{CSH}] - k_w[\text{AlaSEt}] - FvV[\text{AlaSEt}]$$
$$+ [\text{AlaSEt}]_0 FvV$$

$$\frac{d[\text{CSH}]}{dt} = -k_{SS}[\text{CSH}][\mathbf{6}] - k_L[\text{AlaSEt}][\text{CSH}] - k_{mal}[\text{CSH}][\text{Mal}]$$
$$- k_{SS}[\mathbf{7}][\text{CSH}] - FvV[\text{CSH}] + k_{SS}[\text{CSSC}][\text{EtSH}]$$
$$+ k_{SS}[\text{CSSC}][\mathbf{5}]$$

$$\frac{d[\mathbf{5}]}{dt} = -FvV[\mathbf{5}] - k_{SS}[\mathbf{5}][\mathbf{6}] - k_{mal}[\mathbf{5}][\text{mal}]$$
$$- k_{SS}[\mathbf{5}][\text{CSSC}] + k_{SS}[\mathbf{7}][\text{EtSH}]$$
$$+ k_{SS}[\mathbf{7}][\text{CSH}] + k_L[\text{AlaSEt}][\text{CSH}]$$

$$\frac{d[\text{EtSH}]}{dt} = -k_{SS}[\text{CSSC}][\text{EtSH}] - k_{SS}[\mathbf{7}][\text{EtSH}] - k_{mal}[\text{EtSH}][\text{mal}]$$
$$- FvV[\text{EtSH}] + k_{SS}[\text{CSH}][\mathbf{6}] + k_L[\text{AlaSEt}][\text{CSH}]$$
$$+ k_{SS}[\mathbf{5}][\mathbf{6}] + k_w[\text{AlaSEt}]$$

$$\frac{d[\text{CSSC}]}{dt} = -k_{SS}[\text{CSSC}][\text{EtSH}] - k_{SS}[\mathbf{5}][\text{CSSC}] - FvV[\text{CSSC}]$$
$$+ k_{SS}[\text{CSH}][\mathbf{6}] + k_{SS}[\text{CSH}][\mathbf{7}] + FvV[\text{CSSC}]_0$$

$$\frac{d[\mathbf{6}]}{dt} = -k_{SS}[\text{CSH}][\mathbf{6}] - k_{SS}[\mathbf{5}][\mathbf{6}]$$
$$- FvV[\mathbf{6}] + k_{SS}[\text{CSSC}][\text{EtSH}] + k_{SS}[\mathbf{7}][\text{EtSH}]$$

$$\frac{d[\mathbf{7}]}{dt} = -FvV[\mathbf{7}] - k_{SS}[\mathbf{7}][\text{EtSH}] - k_{SS}[\mathbf{7}][\text{CSH}]$$
$$+ k_{SS}[\mathbf{5}][\mathbf{6}] + k_{SS}[\mathbf{5}][\text{CSSC}]$$

$$\frac{d[\text{mal}]}{dt} = -FvV[\text{mal}] - k_{mal}[\text{CSH}][\text{mal}] - k_{mal}[\text{EtSH}][\text{mal}]$$
$$- k_{mal}[\mathbf{5}][\text{mal}] + FvV[\text{mal}]_0 \tag{2}$$

where [mal] is the concentration of maleimide. k_{SS} is the rate constant for all thiol–disulfide interchange reactions; k_L is the rate constant for Kent ligation; k_W is the rate constant for the hydrolysis of AlaSEt; k_{mal} is the rate constant for all conjugate additions of thiols to maleimide; FvV is the space velocity; '0' subscripts indicate concentrations fed into the reactor (constants in our experiments). Under flow conditions, the evolution of the species in the oscillatory network over time is governed by the following set of ordinary differential equations:
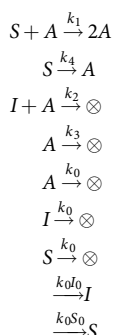
$$\frac{d[\text{AlaSEt}]}{dt} = -k_L[\text{AlaSEt}][\text{CSH}] - k_w[\text{AlaSEt}] - FvV[\text{AlaSEt}]$$
$$+ FvV[\text{AlaSEt}]_0$$

$$\frac{d[\text{CSH}]}{dt} = -k_{SS}[\text{CSH}][\mathbf{6}] - k_L[\text{AlaSEt}][\text{CSH}]$$
$$- k_{mal}[\text{CSH}][\text{mal}] - k_{AAm}[\text{CSH}][\text{AAm}] - k_{SS}[\mathbf{7}][\text{CSH}]$$
$$- FvV[\text{CSH}] + k_{SS}[\text{CSSC}][\text{EtSH}] + k_{SS}[\text{CSSC}][\mathbf{5}]$$

$$\frac{d[\mathbf{5}]}{dt} = -FvV[\mathbf{5}] - k_{SS}[\mathbf{5}][\mathbf{6}] - k_{AAm}[\mathbf{5}][\text{AAm}]$$
$$- k_{mal}[\mathbf{5}][\text{mal}] - k_{SS}[\mathbf{5}][\text{CSSC}] + k_{SS}[\mathbf{7}][\text{EtSH}]$$
$$+ k_{SS}[\mathbf{7}][\text{CSH}] + k_L[\text{AlaSEt}][\text{CSH}]$$

$$\frac{d[\text{EtSH}]}{dt} = -k_{SS}[\text{CSSC}][\text{EtSH}] - k_{SS}[\mathbf{7}][\text{EtSH}] - k_{AAm}[\text{EtSH}][\text{AAm}]$$
$$- k_{mal}[\text{EtSH}][\text{mal}] - FvV[\text{EtSH}] + k_{SS}[\text{CSH}][\mathbf{6}]$$
$$+ k_L[\text{AlaSEt}][\text{CSH}] + k_{SS}[\mathbf{5}][\mathbf{6}] + k_w[\text{AlaSEt}]$$

$$\frac{d[\text{CSSC}]}{dt} = -k_{SS}[\text{CSSC}][\text{EtSH}] - k_{SS}[\mathbf{5}][\text{CSSC}] - FvV[\text{CSSC}]$$
$$+ k_{SS}[\text{CSH}][\mathbf{6}] + k_{SS}[\text{CSH}][\mathbf{7}] + FvV[\text{CSSC}]_0$$

$$\frac{d[\mathbf{6}]}{dt} = -k_{SS}[\text{CSH}][\mathbf{6}] - k_{SS}[\mathbf{5}][\mathbf{6}]$$
$$- FvV[\mathbf{6}] + k_{SS}[\text{CSSC}][\text{EtSH}] + k_{SS}[\mathbf{7}][\text{EtSH}]$$

$$\frac{d[\mathbf{7}]}{dt} = -FvV[\mathbf{7}] - k_{SS}[\mathbf{7}][\text{EtSH}] - k_{SS}[\mathbf{7}][\text{CSH}]$$
$$+ k_{SS}[\mathbf{5}][\mathbf{6}] + k_{SS}[\mathbf{5}][\text{CSSC}]$$

$$\frac{d[\text{mal}]}{dt} = -FvV[\text{mal}] - k_{mal}[\text{CSH}][\text{mal}] - k_{mal}[\text{EtSH}][\text{mal}]$$
$$- k_{mal}[\mathbf{5}][\text{mal}] + FvV[\text{mal}]_0$$

$$\frac{d[\text{AAm}]}{dt} = -FvV[\text{AAm}] - k_{AAm}[\text{CSH}][\text{AAm}] - k_{AAm}[\text{EtSH}][\text{AAm}]$$
$$- k_{AAm}[\mathbf{5}][\text{AAm}] + FvV[\text{AAm}]_0 \tag{3}$$

AAm is acrylamide; k_{AAm} is the rate constant for all conjugate additions of thiols to acrylamide. We numerically solved these two systems of equations (equations (2) and (3)) for the bistable network and oscillatory network for a variety of flow rates, FvV, using a custom code that relies on MATLAB's built-in ode45 algorithm. Selected results of the numerical simulations are shown in Extended Data Figs 5a–c and 6a. Our MATLAB scripts are available as Supplementary Information.

Linear stability analysis of the three-component model of the oscillator. The full oscillator model can be reduced to a three-component model by applying three approximations: first, that the positive feedback loop is described by simple quadratic autocatalysis with rate constant k_1; second, that the negative feedback

loop (reaction with acrylamide) is described by a first-order reaction with rate constant k_3; and third, that the end products can be neglected.

With these assumptions, the system of reactions is described by:

$$S + A \xrightarrow{k_1} 2A$$
$$S \xrightarrow{k_4} A$$
$$I + A \xrightarrow{k_2} \otimes$$
$$A \xrightarrow{k_3} \otimes$$
$$A \xrightarrow{k_0} \otimes$$
$$I \xrightarrow{k_0} \otimes$$
$$S \xrightarrow{k_0} \otimes$$
$$\xrightarrow{k_0 I_0} I$$
$$\xrightarrow{k_0 S_0} S$$

Here $A = [\text{EtSH}] + [\mathbf{5}] + [\text{CSH}] = [\text{RSH}]$, $I = [\text{maleimide}]$, $S = [\text{AlaSEt}]$, k_{1-4} are rate constants and k_0 is the space velocity; $\otimes$ indicated washout or the formation of inactive products; reactions without reactants indicate that the reagents are supplied in the incoming flow. The system of kinetic equations then takes the form of equation (1), reprinted here for convenience:

$$\frac{dA}{dt} = k_1 SA - k_2 IA - k_3 A + k_0 A + k_4 S$$
$$\frac{dI}{dt} = k_0 I_0 - k_0 I - k_2 IA$$
$$\frac{dS}{dt} = k_0 S_0 - k_0 S - k_4 S - k_1 SA$$

To represent the experimental system, we used the following values: $S_0 = 0.05\,\text{M}$, $I_0 = 0.01\,\text{M}$, $k_1 = 0.25\,\text{s}^{-1}\,\text{M}^{-1}$, $k_2 = 300\,\text{s}^{-1}\,\text{M}^{-1}$, $k_3 = 0.0035\,\text{s}^{-1}$ and $k_4 = 7 \times 10^{-5}\,\text{s}^{-1}$. Using these parameters, our numerical model demonstrates sustained oscillations with $k_0 = (1.5-3) \times 10^{-4}\,\text{s}^{-1}$; the region of the sustained oscillations is similar to the region in which sustained oscillations were observed in the experiment.

To describe the experimentally observed dependence of the stability of oscillations on space velocity, we analysed the stability of the steady states derived from the following considerations. The steady states are defined by:

$$\frac{k_1 k_0 S_0 A}{k_0 + k_4 + k_1 A} - \frac{k_2 k_0 I_0 A}{k_0 + k_2 A} - (k_0 + k_3)A + \frac{k_4 k_0 S_0}{k_0 + k_4 + k_1 A} = 0$$

which is equivalent to:

$$0 = (k_1 k_2 k_3 + k_1 k_2 k_0)A^3$$
$$+ [k_0^2(k_1 + k_2) + k_0(k_1 k_2 I_0 + k_2 k_3 + k_2 k_4 + k_1 k_3 - k_1 k_2 S_0) + k_2 k_3 k_4]A^2$$
$$+ [k_0^3 + k_0^2(k_2 I_0 + k_3 + k_4 - k_1 S_0) + k_0(k_2 k_4 I_0 + k_3 k_4 - k_2 k_4 S_0)]A - k_4 k_0^2 S_0$$

The dependence on k_0 for the given rate constants and starting concentrations is then:

$$0 = (0.2625 + 75 k_0)A^3 + (300.25 k_0^2 - 1.928125 k_0 + 7.35 \times 10^{-5})A^2$$
$$+ (k_0^3 + 2.99107 k_0^2 - 8.39755 \times 10^{-4} k_0)A - 3.5 \times 10^{-6} k_0^2$$

The dependence of the roots of this cubic equation on k_0 for the region of interest $(1 \times 10^{-4} < k_0 < 4 \times 10^{-4})$ are shown in the graphs in Extended Data Fig. 8a, b.

An analysis of the discriminant of the cubic equation written above shows that solutions of this equation exhibit a fold bifurcation at $k_0 = 3.08266724620437 \times 10^{-4}\,\text{s}^{-1}$, at which two positive solutions collide and disappear. To analyse the stability of the steady states we use the Jacobian matrix (J), and determine the eigenvalues (λ) such that the following is not invertible:

$$J - \mathcal{I}\lambda = \begin{pmatrix} k_1 S - k_2 I - k_3 - k_0 - \lambda & -k_2 A & k_1 A + k_4 \\ -k_2 I & -k_0 - k_2 A - \lambda & 0 \\ -k_1 S & 0 & -k_1 A - k_0 - k_4 - \lambda \end{pmatrix}$$

where $\mathcal{I}$ is the identity matrix. We used a Mathematica script (Supplementary Information; $x \equiv k_0$, $h_0 \equiv I_0$) to compute the stability of the steady states.

For $k_0 = 3.08266724620437 \times 10^{-4}\,\text{s}^{-1}$ and the steady-state value for A is $[A]_{ss} = 0.0000263986$, the eigenvalues defined by the equation $\det(J - \mathcal{I}\lambda) = 0$ are $\lambda_1 = -0.11456$, $\lambda_2 = -0.000247982$ and $\lambda_3 = -1.59534 \times 10^{-10}$; therefore, λ_3 approaches 0 as is expected for a fold bifurcation.

For $k_0 > 3.08266724620437 \times 10^{-4}\,\text{s}^{-1}$, the lowest steady state is the only stable steady state. For example, for $k_0 = 4 \times 10^{-4}\,\text{s}^{-1}$:

(1) $[A]_{ss} = 3.99596 \times 10^{-6}$ is a stable state ($\lambda_1 = -0.745063$, $\lambda_2 = -0.000453008$ and $\lambda_3 = -0.000407547$ are all negative);

(2) $[A]_{ss} = 0.000242641$ is an unstable state ($\lambda_1 = -0.088553$, $\lambda_2 = -0.000319249$ and $\lambda_3 = 0.00427642$; $\lambda_3 > 0$); and

(3) $[A]_{ss} = 0.00197459$ is an unstable state ($\lambda_1 = -0.594797$, $\lambda_{2,3} = 0.000159607 \mp 0.00128566i$; $\text{Re}(\lambda_{2,3}) > 0$).

For $k_0 < 3.08266724620437 \times 10^{-4}\,\text{s}^{-1}$, there is only one physically meaningful (positive and real) steady state. This steady state undergoes a transition from an unstable focus (eigenvalues are complex conjugates with a positive real part) to a stable focus (eigenvalues are complex conjugates with a negative real part) through an Andronov–Hopf bifurcation (referred to hereafter as a Hopf bifurcation). At the Hopf bifurcation, the real part of the eigenvalues should go through zero and computations show that this is indeed the case (see also Extended Data Fig. 8a):

(i). For $k_0 = 2 \times 10^{-4}\,\text{s}^{-1}$, $[A]_{ss} = 0.00122403$ is an unstable focus, resulting in a stable orbit and sustained oscillations ($\lambda_1 = -0.369038$, $\lambda_{2,3} = 0.0000302409 \mp 0.00112125i$; ; $\text{Re}(\lambda_{2,3}) > 0$).

(ii). For $k_0 = 1.7680658 \times 10^{-4}\,\text{s}^{-1}$, $[A]_{ss} = 0.00111479$ ($\lambda_1 = -0.336194$, $\lambda_{2,3} = 3.55662 \times 10^{-13} \mp 0.00108786i$; $\text{Re}(\lambda_{2,3}) \to 0$ (within the limits of the precision of the computation). This is the point of the Hopf bifurcation.

(iii). For $k_0 = 1.4 \times 10^{-4}\,\text{s}^{-1}$, $[A]_{ss} = 0.00093034$ is a stable focus, resulting in damped oscillations ($\lambda_1 = -0.280744$, $\lambda_{2,3} = -0.0000654976 \mp 0.00102364i$; $\text{Re}(\lambda_{2,3}) < 0$).

Supplementary discussions. *Bifurcations.* A bifurcation point represents a set of conditions for which a smooth change in a control parameter causes a sudden shift in system behaviour. For example, a system might transition from having multiple steady states to having just one, or vice versa (Extended Data Fig. 9b). In our system, as the space velocity is increased to extremely high values, we observe such a transition. The mathematical basis of this transition can be explained by the number of real solutions to a cubic equation ($X^3 - X + C = 0$). These solutions are a function of control parameter C; as C is increased, two out of three real solutions disappear, indicating a bifurcation point.

Oscillatory systems can undergo bifurcations in which they transition from having a single stable steady state to having one unstable steady state with sustained oscillations. This transition, which is called a Poincare–Andronov–Hopf bifurcation, is apparent in our system.

Hysteresis. Hysteresis describes the failure of a system to return to its starting point when an external condition or control parameter is changed and then changed back (Extended Data Fig. 9b). One of the best-known examples of hysteresis is the behaviour of ferromagnetic materials in a magnetic field.

Bistable dynamical systems have at least two stable states (Extended Data Fig. 9b). Without a strong perturbation, the system does not transition from one state to the other. Consequently, when the control parameter is increased from zero, the system will remain at a first set of stable states (the lower solid line in Extended Data Fig. 9b) until a bifurcation point is reached; when the control parameter is again lowered, the system will remain at a second set of stable states (the upper line in Extended Data Fig. 9b) until a bifurcation point is reached. As a result, a hysteresis loop appears.

Detailed chemical explanation. Thioesters are carboxylic acid derivatives that can react with various nucleophiles through nucleophilic substitution at their sp^2 carbon. Such a reaction consists of two steps: addition of the nucleophile and loss of the leaving group (for example, thiolate). Our system contains AlaSEt as the thioester and three nucleophiles (hydroxyl, amines and thiolates) with which it can react to form alanine (carboxylic acid), amides and new thioesters (reaction with thiolate is also called thiol–thioester exchange). At pH 7.5–8, reactions with hydroxyls and amines are slow, and reactions with thiolate are fast[36] but reversible (the product is another thioester). Kent ligation relies on this difference in reaction rates. Thiol–thioester exchange goes quickly and is followed by a quick, entropically favourable intramolecular reaction with amine.

In our autocatalytic pathway, CSH reacts with AlaSEt through Kent ligation. This ligation is followed by a fast thiolate–disulfide reaction, making the complete autocatalytic process fast[37], relative to other reactions in our system.

Two independent pathways result in alanine amides in our system: the direct reaction of amines from CSSC, a noncatalytic reaction, and an autocatalytic pathway through CSH. The ratio between these two pathways is 1:100 or more for our system and is responsible for enabling fine control over the autocatalytic process.

If we run an autocatalytic reaction in a CSTR, then two new processes are added: the continuous addition of thioester and disulfide through the inlet and the removal of thiols and all other products through an outlet (removal of thiols slows amplification). The final concentration of thiols represents a balance between these two processes and the aforementioned reactions.

Maleimide is a conjugated carbonyl derivative, with which nucleophiles can readily react through conjugate addition (that is, addition to the double bond next to the carbonyl group). Maleimide reacts with thiols much faster than with thioesters and disulfides involved in the autocatalytic process and, hence, gives rise to two steady states in a CSTR. In the first state, which has very low concentrations of thiols, maleimide is supplied by flow faster than it is removed by reaction with thiols. In the second state, which has very high concentrations of thiols produced through the autocatalytic pathway, maleimide is consumed by thiols faster than it is supplied by flow.

The addition of acrylamide leads to oscillations. Acrylamide, similarly to maleimide, is a conjugated carbonyl compound that reacts with the same nucleophiles as maleimide. However, its reactivity is several orders of magnitude lower than that of maleimide; as a result, acrylamide is not able to suppress the autocatalytic pathway and is able to remove thiols only when the thioester is depleted. The mechanism by which the slow removal of an activator (that is, the slow removal of thiols by acrylamide) converts a bistable system into an oscillatory system is described in detail in ref. 13. Briefly, acrylamide creates a mechanism of negative feedback—as the concentration of thiols is increased, their rate of acrylamide-mediated removal increases—which destabilizes the high-thiol steady state leaving only an unstable state at low flow rates. The system is forced to oscillate around this unstable state.

31. Haynes, W. M. (ed.) *Handbook of Chemistry and Physics* 5-88–5-97 (CRC, 2015).
32. Nikolsky, B. P. (ed.) *Chemical Handbook* Vol. 3, 85–105 (Chimia, 1971).
33. Benesch, R. E. & Benesch, R. The acid strength of the –SH group in cysteine and related compounds. *J. Am. Chem. Soc.* **77,** 5877–5881 (1955).
34. Whitesides, G. M., Lilburn, J. E. & Szajewski, R. P. Rates of thiol-disulfide interchange reactions between mono- and dithiols and ellmans reagent. *J. Org. Chem.* **42,** 332–338 (1977).
35. Hoops, S. *et al.* COPASI—a complex pathway simulator. *Bioinformatics* **22,** 3067–3074 (2006).
36. Bracher, P. J., Snyder, P. W., Bohall, B. R. & Whitesides, G. M. The relative rates of thiol-thioester exchange and hydrolysis for alkyl and aryl thioalkanoates in water. *Orig. Life Evol. Biosph.* **41,** 399–412 (2011).
37. Steinfeld, J. I., Francisco, J. S. & Hase, W. L. *Chemical Kinetics and Dynamics* 2nd edn, Ch. 5, 151–152 (Prentice Hall, 1999).
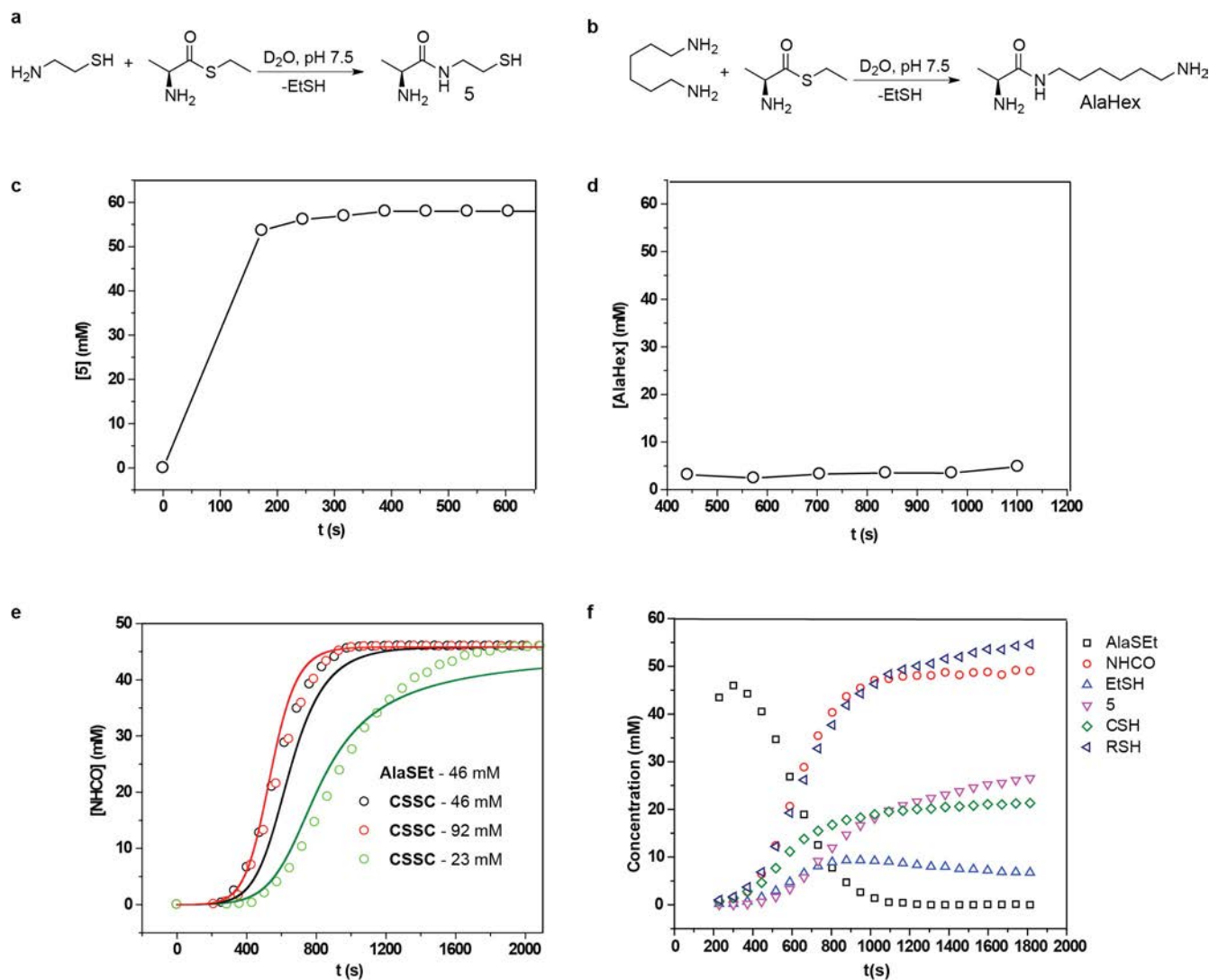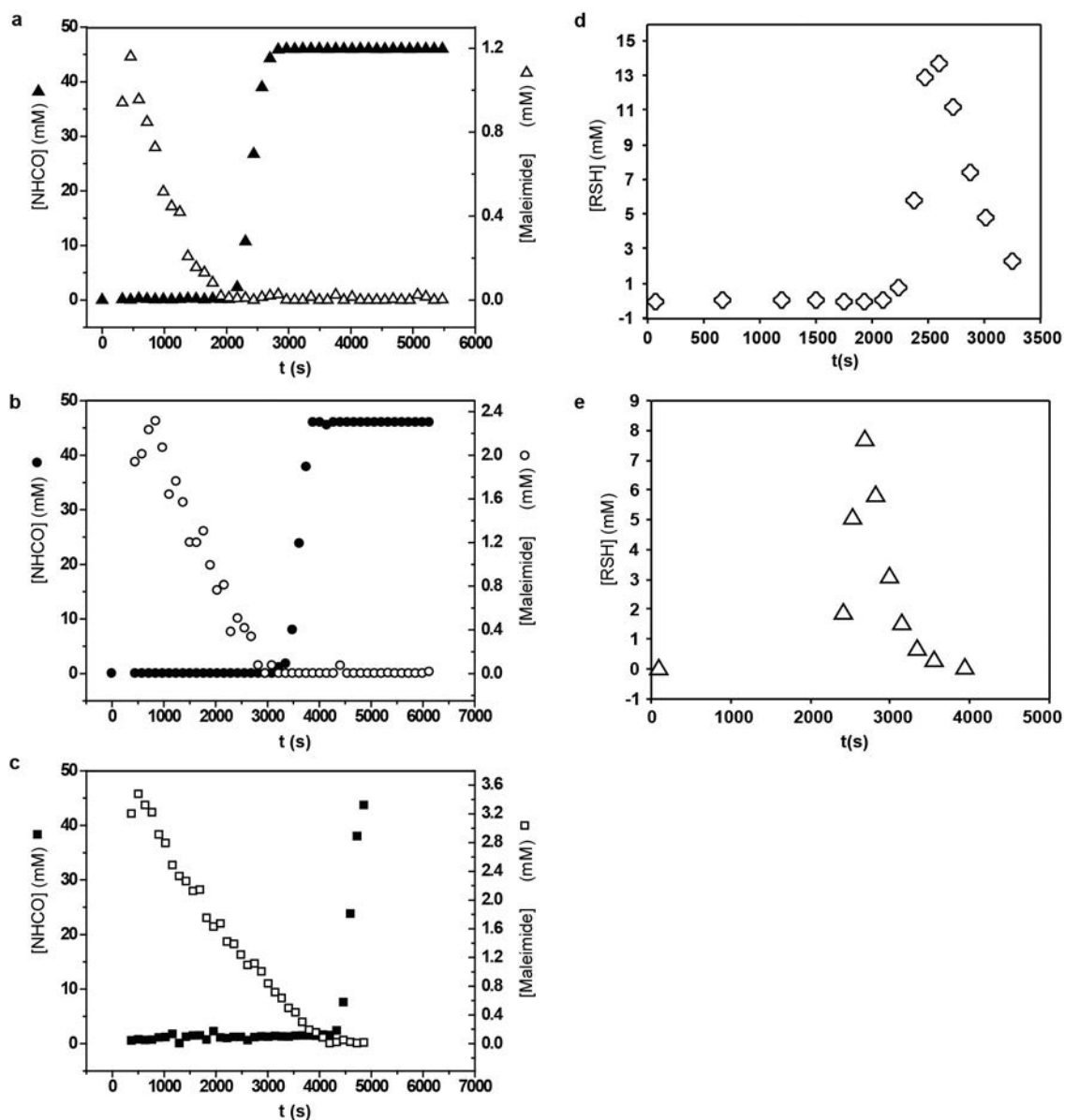
Extended Data Figure 1 | ^{1}H NMR kinetic experiments showing the mechanism for autocatalysis in AlaSEt with CSSC reaction. a, Scheme for the reaction between AlaSEt and CSH. **b**, Scheme for the reaction between AlaSEt and hexamethylendiamine. **c**, Kinetic plot for the reaction between AlaSEt and CSH. Reaction conditions: D$_2$O, pH 7.5, 500 mM phosphate buffer, 25 °C, AlaSEt (58 mM), CSH (88 mM). **d**, Kinetic plot for the reaction between AlaSEt and hexamethylendiamine. Reaction conditions: D$_2$O, pH 7.5, 500 mM phosphate buffer, 25 °C, AlaSEt (58 mM), hexamethylendiamine (88 mM). **e**, Kinetic plot for our autocatalytic thiol network. Reaction conditions: 500 mM phosphate buffer pH 7.5, 25 °C, D$_2$O. Points represent experimental data and solid

lines represent the predictions of numerical simulations of the system. We assume the following: all disulfide–thiol interchange reactions proceed with the same rate constant $k_{SS} = 0.65$ s^{-1} M^{-1}; Kent ligation proceeds with rate constant $k_L = 0.41$ s^{-1} M^{-1}; and hydrolysis proceeds with rate constant $k_w = 7.00 \times 10^{-6}$ s^{-1}). The poor fit of the experiment with [CSSC] = 23 mM is a result of a simplifying assumption that all thiolate–disulfide interchanges in the model occur with equal rate constants in the forward and reverse directions. **f**, Time profiles for selected individual compounds in the autocatalytic thiol network. Reaction conditions: 500 mM phosphate buffer pH 7.5, 25 °C, D$_2$O, [AlaSEt] = 46 mM, [CSSC] = 46 mM.
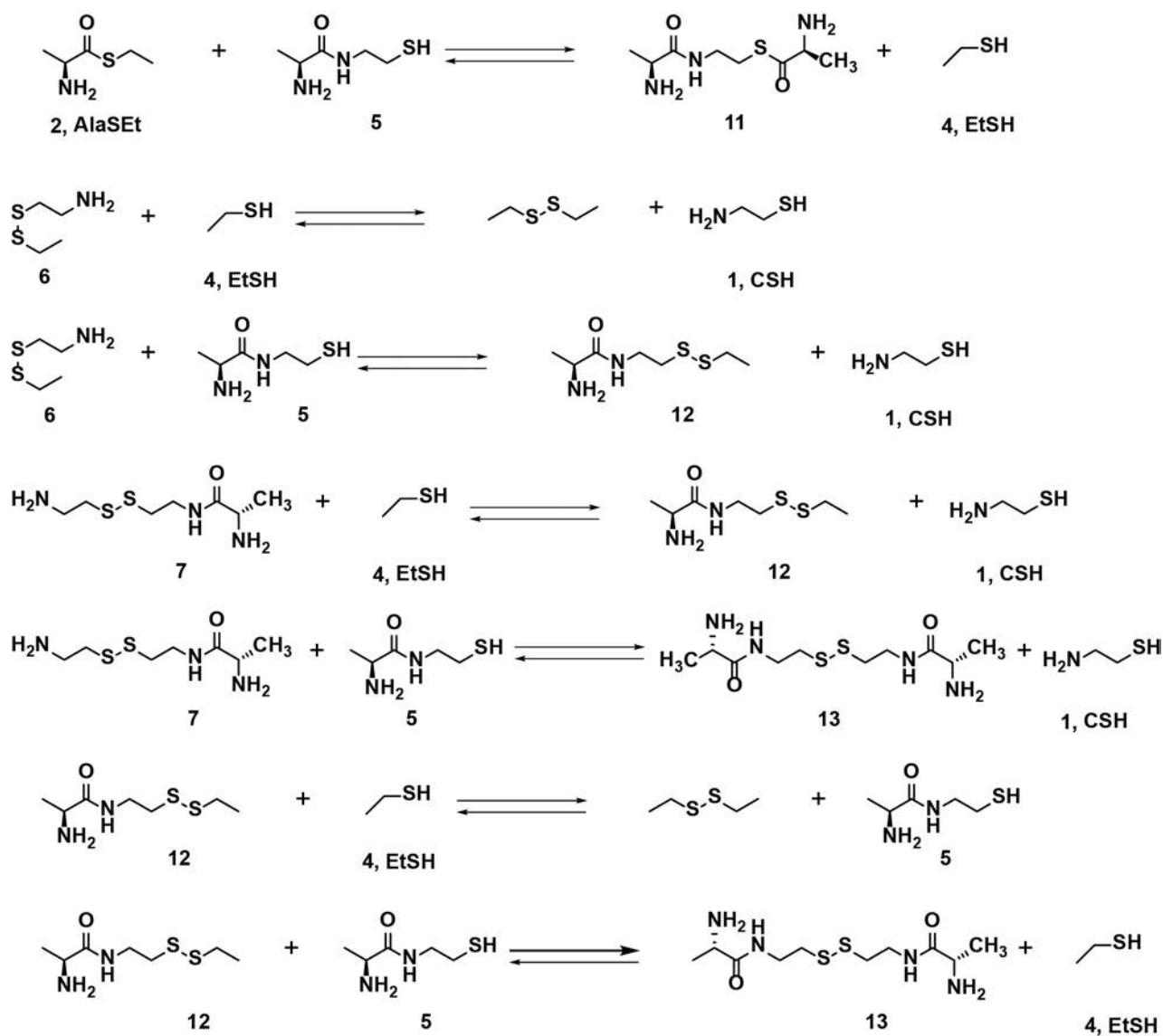
Extended Data Figure 2 | Schematic representation of the thiol–disulfide interchange reactions and thiol–thioester exchange reactions.
The thiol–thioester exchange reactions are those that we omitted from Fig. 1b because they do not significantly alter the dynamics of the system.

Extended Data Figure 3 | Batch kinetic experiments. a–c, Kinetics plots for the reaction of AlaSEt with CSSC and maleimide. Reaction conditions: 500 mM phosphate buffer pH 7.5, 25 °C, D_2O, [AlaSEt] = 46 mM, CSSC = 46 mM, [maleimide] = 1.16 mM (**a**), 2.31 mM (**b**) or 3.47 mM (**c**). **d**, **e**, Kinetics plots for batch reaction between AlaSEt, CSSC, maleimide and acrylamide. Reaction conditions: 1 M phosphate buffer pH 8, 25 °C, H_2O, [AlaSEt] = 46 mM, [CSSC] = 92 mM, [maleimide] = 10 mM, [acrylamide] = 160 mM (**d**) or 320 mM (**e**).
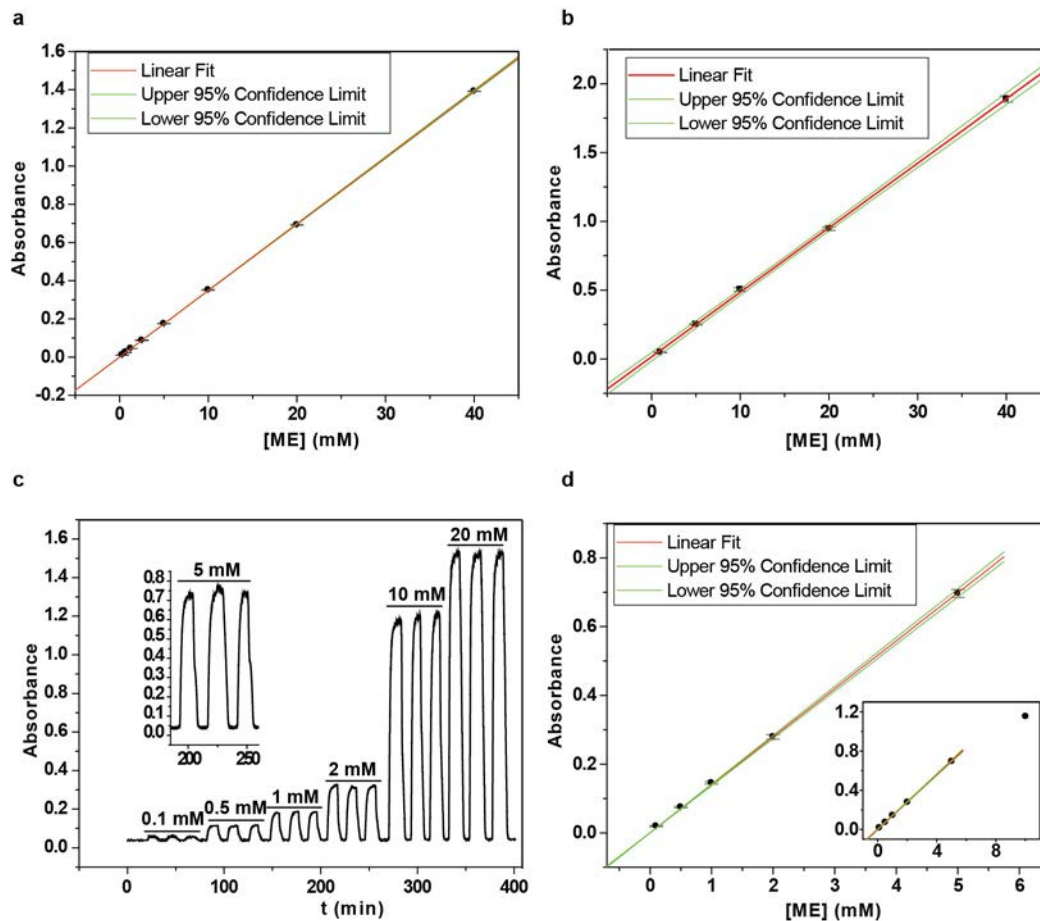
Extended Data Figure 4 | Calibration curves for the determination of the total concentration of free thiols. a, Calibration curve for the batch experiments; $[RSH] = A \times 28.71$ mM, where A stands for absorbance. **b**, Calibration curve for the detection system in which a microfluidic chip was coupled to the fibre optic spectrophotometer; $[RSH] = (A - 0.01496) \times 21.32$ mM. **c**, Trace of the absorbance from the calibration experiment for the detection system in which a glass flow cell was coupled to the Cary 60 ultraviolet–visual spectrophotometer;

$[RSH] = (A - 0.03848) \times 7.16$ mM. The concentrations above the lines show β-mercaptoethanol (ME) concentrations used for getting responses in absorbance under the line. The inset shows a separate experiment where 5 mM of ME were used. **d**, Calibration curve that was obtained from the data in **c**. The inset demonstrates loss of linearity of the calibration curve above approximately 8 mM of ME. Error bars in **a, b** and **d** correspond to 95% confidence intervals calculated using Student's t-test (three independent experiments for each point).
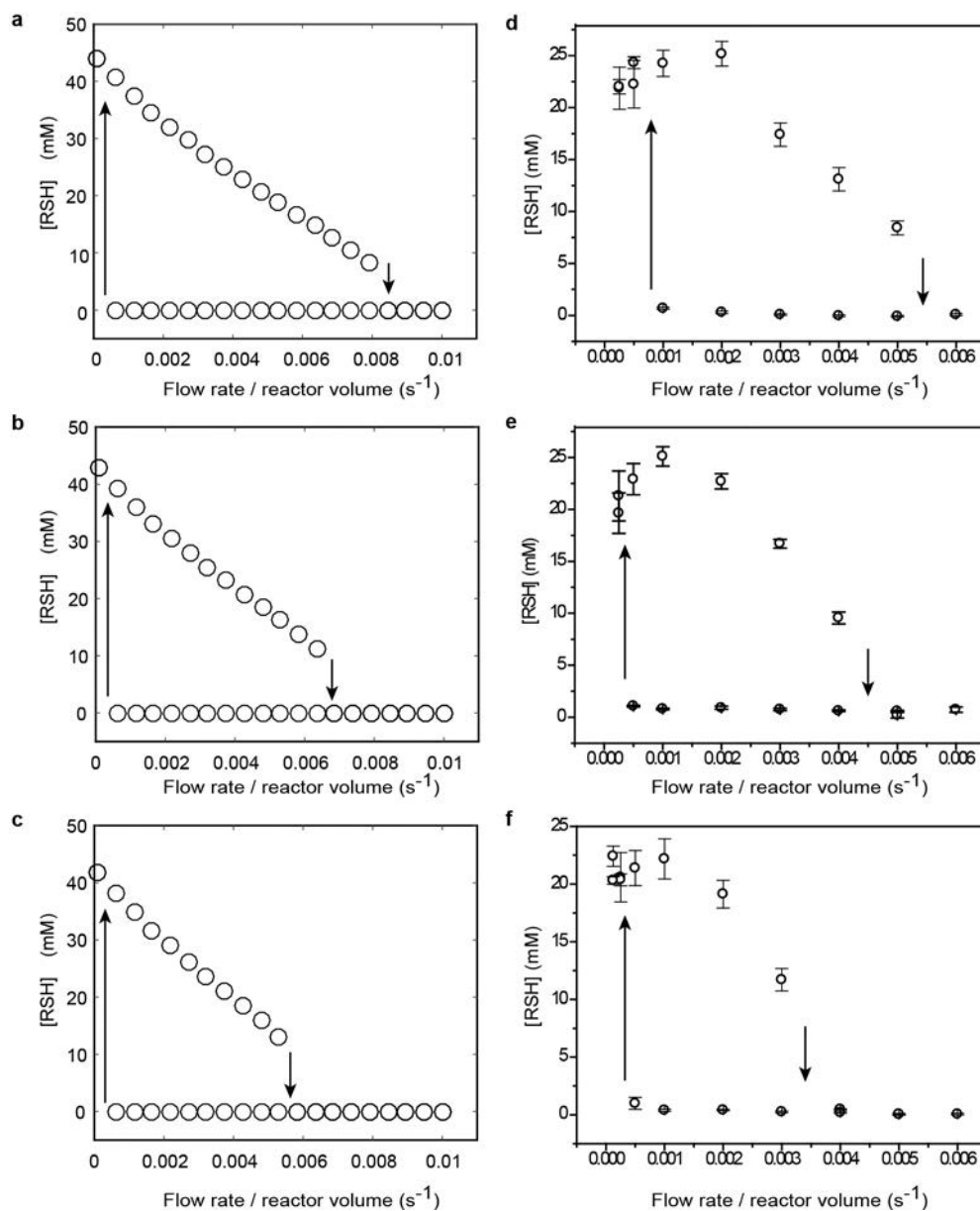
Extended Data Figure 5 | Bistability in the maleimide delayed autocatalytic thiol network. a–c, Modelling of the hysteresis in the maleimide delayed autocatalytic thiol network in a CSTR with the following parameters: $k_{SS} = 0.65\ s^{-1}\ M^{-1}$, $k_L = 0.41\ s^{-1}\ M^{-1}$, $k_w = 9.26 \times 10^{-6}\ s^{-1}$, $k_{mal} = 150\ s^{-1}\ M^{-1}$, $[CSSC]_0 = 100\ mM$, $[AlaSEt]_0 = 50\ mM$, $[mal]_0 = 1.16\ mM$ (**a**), 2.31 mM (**b**) or 3.47 mM (**c**). **d–f**, Hysteresis curves for bistability experiments with different maleimide

concentrations. Reaction conditions: 0.5 M phosphate buffer pH 7.5, 25 °C, $[AlaSEt] = 47\ mM$, $[CSSC] = 92\ mM$, $[maleimide] = 1.16\ mM$ (**d**), 2.31 mM (**e**) or 3.47 mM (**f**). In all panels, arrows indicate the direction of change. Error bars in **d**, **e** and **f** correspond to standard deviations that were calculated from data points ($n > 100$) in the time intervals that were used to determine the steady-state values of [RSH] for each space velocity.
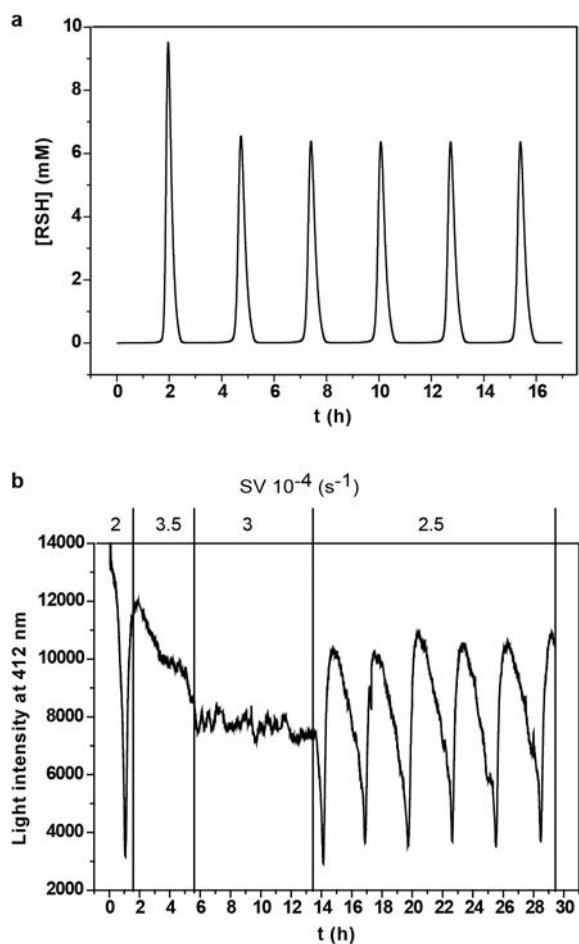
Extended Data Figure 6 | Identification of space velocities resulting in sustained oscillations. a, Numerical simulations predicting sustained oscillations based on the following parameters: $k_{SS} = 0.444 \text{ s}^{-1} \text{M}^{-1}$, $k_L = 0.46 \text{ s}^{-1} \text{M}^{-1}$, $k_w = 6.64 \times 10^{-5} \text{ s}^{-1}$, $k_{mal} = 150 \text{ s}^{-1} \text{M}^{-1}$, $k_{AAm} = 0.014 \text{ s}^{-1} \text{M}^{-1}$, $[CSSC]_0 = 100 \text{ mM}$, $[AlaSEt]_0 = 50 \text{ mM}$, $[mal]_0 = 10 \text{ mM}$, $[acrylamide]_0 \equiv [AAm]_0 = 290 \text{ mM}$ (see Methods), space velocity $SV = 0.0002 \text{ s}^{-1}$. **b**, Adjustment of the flow rate in the oscillatory experiments. Reaction conditions: 1 M phosphate buffer pH 8, $[AlaSEt] = 47 \text{ mM}$, $[CSSC] = 92 \text{ mM}$, $[maleimide] = 10.3 \text{ mM}$, $[acrylamide] = 321 \text{ mM}$.
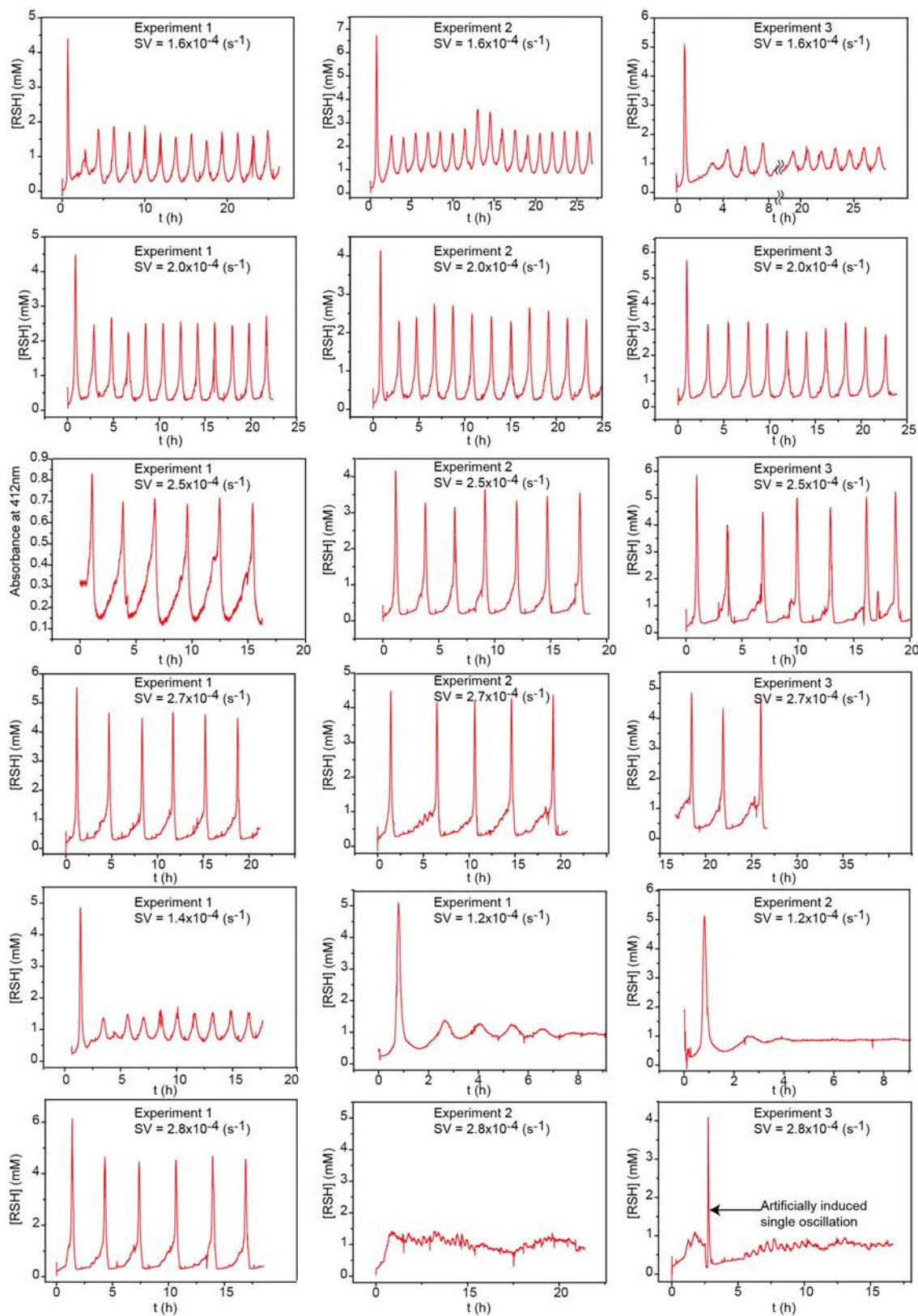
Extended Data Figure 7 | Summary of all oscillatory experiments.
Reaction conditions: 1 M phosphate buffer pH 8, [AlaSEt] = 47 mM,
[CSSC] = 92 mM, [maleimide] = 10.3 mM, [acrylamide] = 321 mM.
The qualitatively different behaviour of the system at space velocity
$SV = 2.8 \times 10^{-4}\,s^{-1}$ (bottom row) is an indication of the bifurcation point.
The apparent thiol concentration of 0.5–1 mM in experiments 2 and 3 at
this space velocity is the result of a background reaction of AlaSEt with
Ellman's reagent that occurs with a rate constant that is about 4×10^{4}
times slower than the reported apparent second-order rate constant of
the reaction between Ellman's reagent and β-mercaptoethanol at
pH 7 (ref. 36).
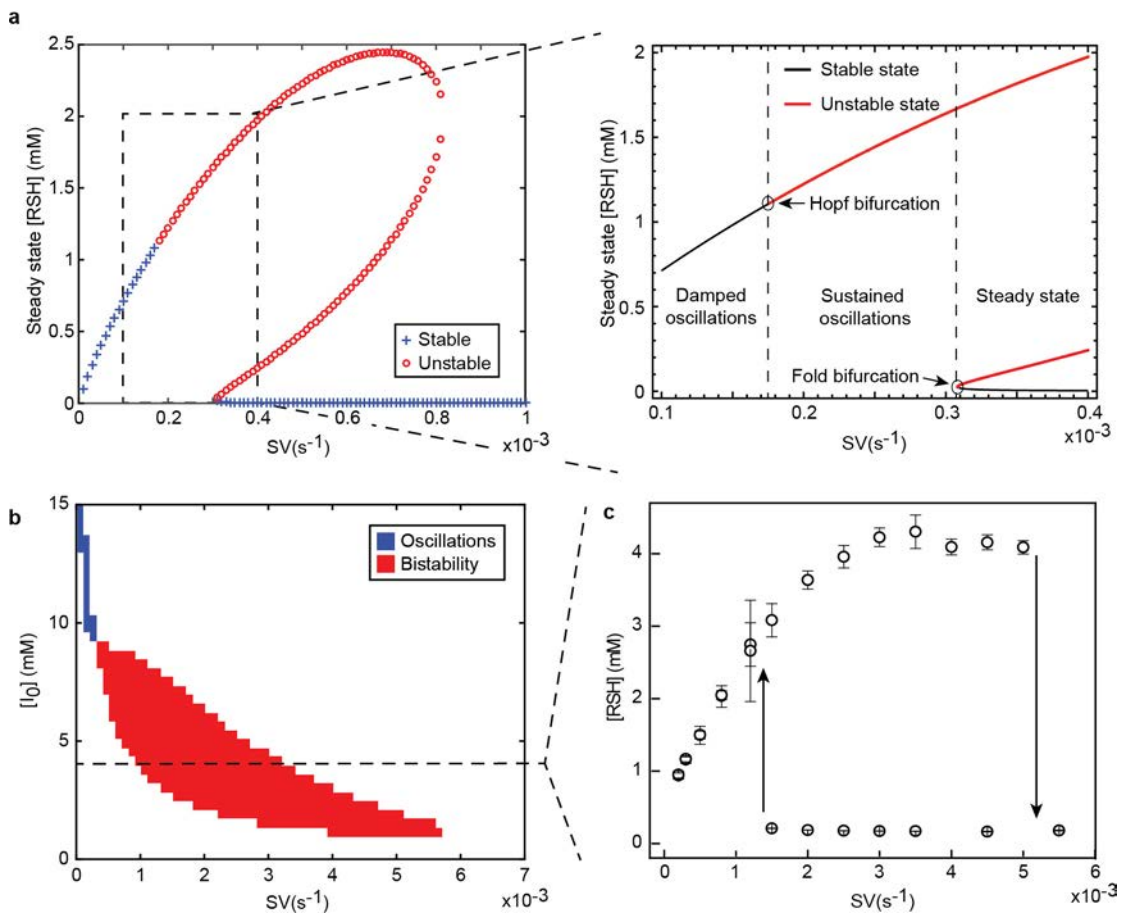
Extended Data Figure 8 | Analysis of for the three-component model.
a, Results of the linear stability analysis of the three-component
model. The graphs show steady states, which were calculated from the
model (equation (1); with $S_0 = 0.05$ M, $I_0 = 0.01$ M, $k_1 = 0.25$ s^{-1} M^{-1},
$k_2 = 300$ s^{-1} M^{-1}, $k_3 = 0.0035$ s^{-1} and $k_4 = 7 \times 10^{-5}$ s^{-1}), and their stability.
In this model, k_0 is the space velocity (SV). The right panel shows detailed
analyses of the region indicated by the dashed square in the left panel.
Details of the linear stability analysis is provided in Supplementary
Information. **b**, A phase plot computed from the three-component
model. **c**, Experimental hysteresis plot demonstrating the transition from
oscillations to bistability with lowering of the feeding concentration of
maleimide; arrows indicate the direction of change. Error bars correspond
to standard deviations calculated from data points ($n > 100$) in the time
intervals that were used to determine the steady-state values of [RSH]
for each space velocity. Reaction conditions: 1 M phosphate buffer
pH 8, 25 °C, [AlaSEt] = 47 mM, [CSSC] = 92 mM, [maleimide] = 4 mM,
[acrylamide] = 321 mM. Dashed line shows correspondence between the
maleimide concentration and the range space velocities on the phase plot
and in the experiment.
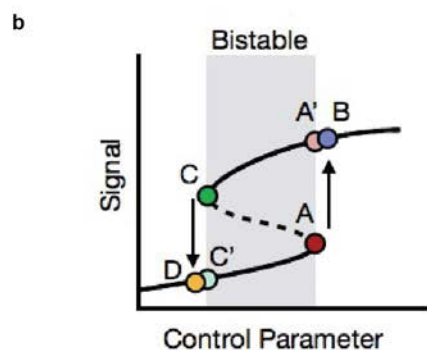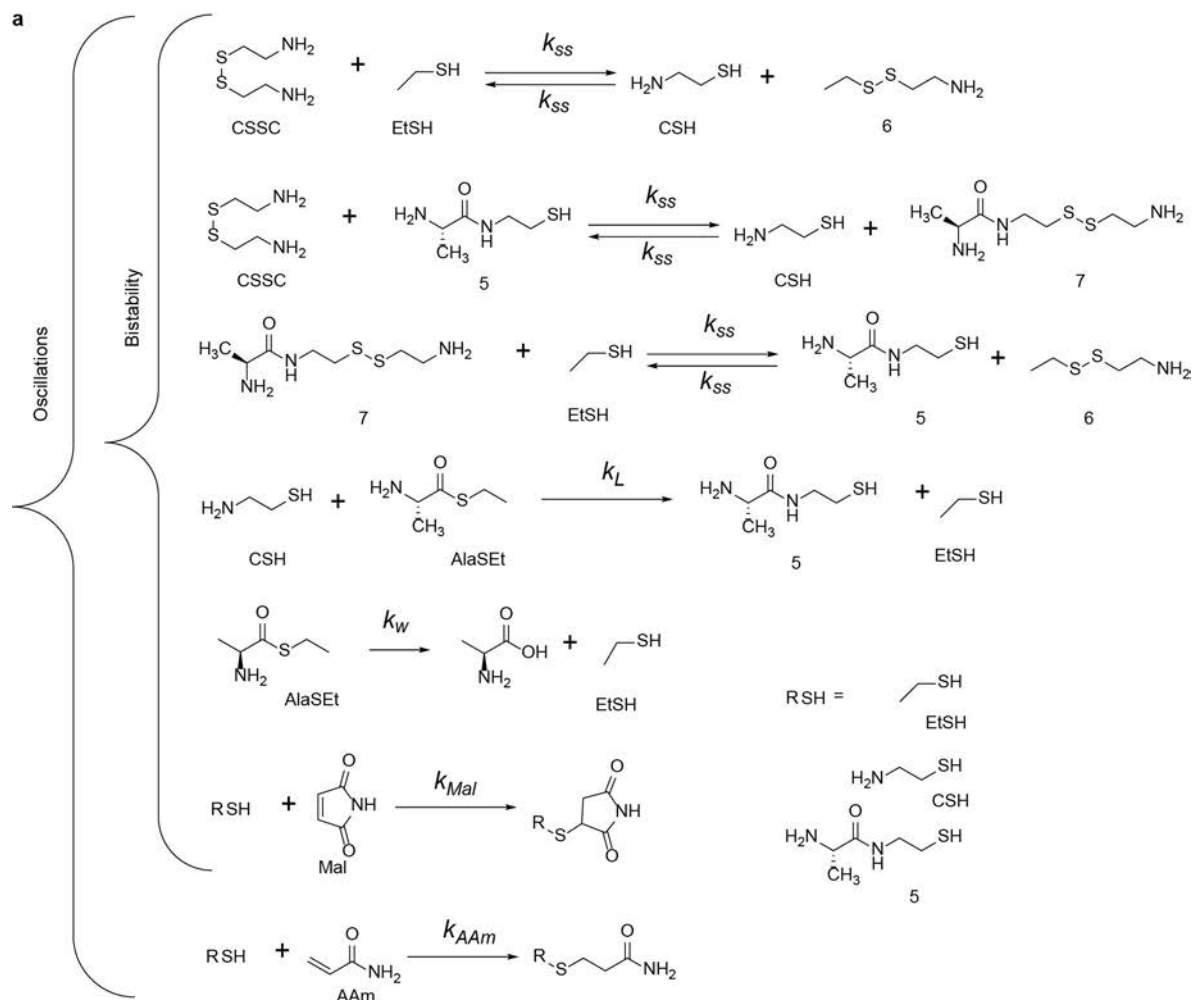
Extended Data Figure 9 | Details of the full numerical model and an illustration of bistability and hysteresis. a, Schematic representation of the reactions that were considered in the full models of the bistable network and the oscillatory network. **b**, An example of a fold bifurcation. As the control parameter is increased, the system transitions from having two stable states (A and A′) to having just one (B). The transition from A to B is often called a critical transition. After the transition, lowering the control parameter will not return the system to A. This phenomenon is called hysteresis. When the control parameter is lowered sufficiently, the system will again transition from having two stable states (C and C′) to having just one (D).

Extended Data Table 1 | pK_a values for the most important thiol and amino derivatives, and estimated populations of different species at equilibrium

Compound	pKa	pH 7.5	pH 8
CSH	10.5; 8.3 [31]	$NH_3^+CH_2CH_2SH$ (84.5 %)	65.0 %
		$NH_3^+CH_2CH_2S^-$ (9.7 %)[#]	23.3 %
		$NH_2CH_2CH_2SH$ (4.8 %)[#]	11.6 %
		$NH_2CH_2CH_2S^-$ (0.01 %)	0.1 %
CSSC	9.0 ± 0.1*	$(NH_3^+CH_2CH_2S)_2$ (96.7 %)	90.3 %
		$(NH_2CH_2CH_2S)_2$ (3.3 %)	9.7 %
AlaSEt	7.4 ± 0.3*	$NH_3^+CH(CH_3)COSC_2H_5$ (46.5 %)	21.6 %
		$NH_2CH(CH_3)COSC_2H_5$ (53.5 %)	78.4 %
EtSH	10.5 [32]	C_2H_5SH (99.9 %)	99.7 %
		$C_2H_5S^-$ (0.1 %)	0.3 %
5	8.2 ± 0.3,	$NH_3^+CH(CH_3)CONH(CH_2)_2SH$ (83.8 %)	62.5 %
	9.7 ± 0.1*	$NH_3^+CH(CH_3)CONH(CH_2)_2S^-$ (0.7%)†	1.2 %
		$NH_2CH(CH_3)CONH(CH_2)_2SH$ (15.4 %)†	35.6 %
		$NH_2CH(CH_3)CONH(CH_2)_2S^-$ (0.1 %)	0.7 %
Ala	9.7 [31]	$NH_3^+CH(CH_3)COO-$ (99.4 %)	98.1 %
		$NH_2CH(CH_3)COO-$ (0.6 %)	1.9 %

Some data are from refs 31 and 32, as shown.
*Values were calculated using ACDLabs software available through SciFinder (Advanced Chemistry Development version 11.02; https://scifinder.cas.org/).
#Values are based on data for the ratio between the neutral and zwitterionic forms for cysteine from ref. 33.
†Calculations are based on the approximation that protonation of the amine group and deprotonation of the thiol group are fully independent processes; that is, for example, the thiol pK_a of the thiol group of $NH_3^+CH(CH_3)CONH(CH_2)_2SH$ and the thiol group of $NH_2CH(CH_3)CONH(CH_2)_2SH$ are the same.